Remote Sensing Derived Products For Precision Farming

Clinton '99 Report

Natural Ressources
Canada

Ressources naturelles
Canada

Canada Centre for
Remote Sensing

Centre canadien
de télédétection
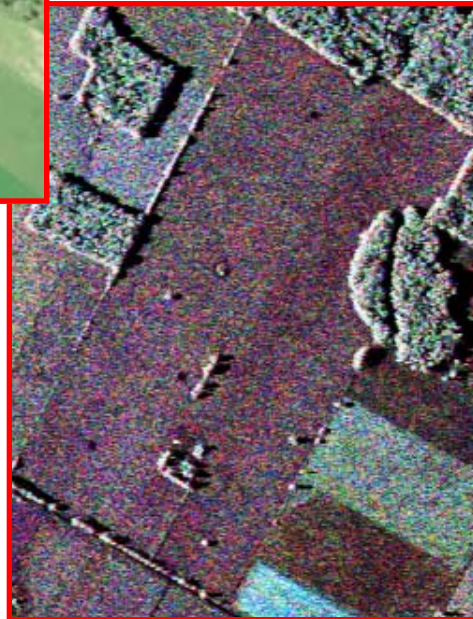
Heather McNairn
Jean-Claude Deguise
Anna Pacheco

Applications Division
Canada Centre for Remote Sensing
Natural Resources Canada

November 1, 2001

Table of Contents

1. Overview of Clinton '99 Project

1.1 *Participants in Clinton '99*

The Clinton 1999 project was a collaborative research and development initiative undertaken by the Canada Centre for Remote Sensing (CCRS) in collaboration with Cargill and Agri-food Laboratories (AFL). A list of project participants and contact information is provided in Table 1. Cargill is an international marketer, processor and distributor of agricultural, food, financial and industrial products and services. The company has 85,000 employees in 60 countries (see http://www.cargill.com/). The Cargill office situated in Clinton, Ontario was involved in this research project. Agri-Food Laboratories is the largest independently owned agricultural facility in Ontario (see http://www.agtest.com/). They provide analytical services for feed, soil and water as well as quality control testing for agricultural manufacturing of feed and fertilizer. AFL has two offices – one in Guelph, and a second office dealing with GIS mapping in Embro, Ontario.

The Geography Department of the University of Ottawa was also involved in the data collection and analysis during the Clinton '99 project. These data are supporting the M.S. thesis work of two students at the University.

Table 1. List Of Participants And Contact Information

	Telephone	*Email*
CCRS (588 Booth St., Ottawa ON K1A 0Y7)		
Jean-Clause Deguise	613-947-1229	Jean-Claude.Deguise@geocan.nrcan.gc.ca
Heather McNairn	613-947-1815	heather.mcnairn@ccrs.nrcan.gc.ca
Anna Pacheco	613-947-1364	anna.pacheco@ccrs.nrcan.gc.ca
Karl Staenz	613-947-1250	karl.staenz@ccrs.nrcan.gc.ca
Cargill (R.R. #4 Clinton, ON N0M 1L0)		
Susan Bird		
Dennis O'Connor	519-233-3423	dennis.oconnor@odyssey.on.ca
AFL Mapping Center (110 Huron St., P.O. Box 162, Embro, ON N0J 1J0)		
Dale and Karon Cowan	519-475-6878	karon@agtest.com
University of Ottawa (60 University St., P.O. Box 450, Stn. A, Ottawa, ON K1N 5N5)		
Abdou Bannari	613-562-5800 ext.1042	abannari@uottawa.ca
Catherine Champagne		catherine.champagne@ccrs.nrcan.gc.ca

1.2 *Hyperspectral and Synthetic Aperture Radar Imagery for Use in Precision Farming*

Significant spatial and temporal variability is associated with both soil and crop characteristics. Measuring and monitoring these characteristics using traditional ground

surveys can often be prohibitive because of the time and cost of data acquisition and processing. Acquisition of data from remote sensors on aircraft or satellite platforms offers an alternative. These data are acquired over large areas and in the case of orbiting satellites, data are provided continuously throughout the growing season. However, extracting meaningful quantitative information from the data is a challenge and the application of remote sensing imagery to precision farming is still being investigated.

Optical sensors record the reflectance of visible (400-700 nm) and infrared (700-2500 nm) electromagnetic energy. Energy in these regions of the spectrum is sensitive to the plant pigmentations and internal leaf structure of vegetation. Multispectral sensors like SPOT and Landsat record reflectance in a few very broad spectral bands. In contrast, hyperspectral sensors record reflected energy in many narrow and contiguous spectral bands. With these characteristics, hyperspectral sensors are often able to detect very specific reflectance and absorption features associated with the imaged target. As a result, these sensors provide a unique opportunity to extract quantitative biophysical and biochemical information about the target.

The application of remote sensing to crop monitoring requires frequent coverage and often requires data acquisitions during specific critical crop phenological stages. Cloud cover can be an impediment to the operational application of remote sensing to precision farming. Microwave instruments like Synthetic Aperture Radars (SARs) operate at much longer wavelengths (~ 0.01 m to 15 m) in comparison to optical sensors. These longer wavelengths are generally not affected by the atmosphere and as such, can acquire imagery regardless of cloud cover. In the microwave region of the electromagnetic spectrum, it is the large-scale structure and dielectric properties (water content) of the target that primarily influences the amount of energy scattered back towards the sensor. Microwaves also penetrate much further into the crop canopy and the soil relative to energy at optical wavelengths. Thus radar and optical sensors respond to very different crop and soil characteristics, and information from these two data sources is considered complementary.

1.3 *Objectives of Clinton '99*

Prior to the formulation of the data acquisition plan and the execution of the experiment, CCRS, Cargill and AFL agreed to a list of research objectives. These are listed below.

Science Objectives:
- Validation of pixel endmember fractions derived from spectral unmixing methods:
  - What exactly does a fraction represent in the field?
  - What is the relationship between vegetation fractions and indicators of crop vigor (LAI, biomass, …)?
  - How many bands of imagery do we really need to extract spectral unmixing information?

- Mapping location (and possibly) type of weeds to identify and mitigate against weed escapes:
  - Weed spectral library (from field spectroradiometer) of different weed types will be compiled.

- Validation of biophysical parameters measured with existing methods:
  - Canopy liquid water content (equivalent water thickness)
  - Leaf Area Index

- Acquisition of field data for the development and validation of new semi-empirical models for deriving biophysical crop parameters:
  - Chlorophyll
  - Leaf nitrogen content
  - Soil nutrient levels
  - Soil moisture

- Simulate multispectral products of future high-spatial resolution satellites and demonstrate their potential for precision agriculture:
  - Can biophysical parameters and unmixing results be derived using imagery simulated to match the specifications of future satellites?
    - Ikonos 2
    - Resource 21
    - Xstar

- Evaluate the applicability of SAR data for precision agriculture:
  - Can RADARSAT-2 "Ultra-Fine" Mode 3m data provide site specific information?

- To further evaluate RADARSAT-2 configurations (HH, VV, HV) for crop condition assessment
  - How sensitive is multi-polarized data to indicators of crop vigor (LAI, biomass)?

- Address the synergy of SAR and high spatial optical data
  - Can SAR data fill the gaps when optical data are not available?

- Acquire field and remote sensing data required in growth and yield modeling (TBD)

Operational Objectives:

- To develop field ready, saleable remote sensing products for the farm level. Remote sensing data products might be useful to the agricultural service industry by helping to direct crop scouting activities and by aiding in the planning of sampling and management strategies for clients. Producers might themselves be interested in weed

and nutrient maps that could be used with variable rate applicators to site specifically direct herbicide and fertilizer inputs.

2. Description of the Data Acquisition

2.1 *Site and Field Descriptions*

The study site was approximately centred on the town of Clinton, in southern Ontario (Canada) (43° 40' N; 81° 30' W) (Figure 1). Crops in this agricultural region are composed mainly of beans, corn, forage crops and small grains (wheat and barley).

Figure 1. Study Site Location: Clinton, Ontario (Canada)

Within this general study site, six fields were chosen for intense sampling. These fields included three white bean fields as well as three corn fields. These fields belong to clients of Cargill and AFL, and these companies were providing sampling, mapping and scouting services over these fields. In addition to these six fields, two additional wheat fields were used in the analysis of the radar imagery. AFL identified these wheat fields after their review of the radar "quicklook" imagery. AFL observed patterns in the radar imagery similar to patterns in the yields maps. Details of these eight fields are given in Table 2.

Four of the six bean and corn fields were considered primary sites and two fields were back-up fields. On the four primary fields, double seeded, weed, residue and bare patches were planned. These patches were located in different soil zones within the fields, where variability in soil and vegetation characteristics among the patches would be maximized. Each patch was approximately 20 m by 20 m in dimension (Figure 2). The perimeter of

each patch was walked with a Differential GPS unit. These patches were used in the processing of manually selecting endmembers for input into spectral unmixing. Details of these patches, for each field, are described below.

Table 2. Description Of Clinton '99 Fields

Field Name	Crop Type	Location	Rank	Details
Forbes	Corn	Lot 29 Con 6 Hullett	Primary	• in hay for the last 5 years • will have a large perennial weed spectrum • has significant topography • approximately 75 acres
Pig Barn	Corn	Lot 35 Con 5 McKillop	Primary	• has had a perennial weed problem, primarily with nutsedge • partly manured in the spring • in soybeans in 1997 and wheat in 1998 • approximately 73 acres
Wright	Corn	Lot 2 Con 3 Hullett	Backup	• approximately 90 acres
Montgomery	White Beans	Lot 41 Con 7 East Wawanosh	Primary	• has a potential for white mould (based upon manure application) or for insect damage • significant corn residue • approximately 75 acres
Sigma	White Beans	Lot 38 Con 3 East Wawanosh	Primary	• in wheat in 1996, soybeans in 1997 and corn in 1998 • has a downward slope from south to north • significant corn residue (no-till) • approximately 65 acres
Vanderyk	White Beans		Backup	• approximately 47 acres
Carter	Red Wheat			• used in radar analysis only
Eckert	White Wheat			• used in radar analysis only

Forbes:
- Two bare patches
- Two weed patches
- Two double seeded patches

Pig Barn:
- Three bare patches
- One weed patch

Montgomery
- Three bare patches
- One double seeded patch
- One residue patch

Sigma
- Three bare patches

Figure 2. Soil And Residue Patches On The Fields

a) Soil Patch In Forbes

b) Residue Patch In Montgomery

In addition to these eight quantitative fields, qualitative crop information was gathered on about 300 fields within the study site. Crop type, growth stage and row direction information was recorded for each field. Field locations were indicated on air photos acquired over the study site.

2.2 *Remote Sensing Acquisitions*

Hyperspectral image data were acquired over the Clinton area on July 7th 1999 using the airborne Probe-1 sensor (Earth Search Sciences Inc., 2001) (Figure 3). The Probe-1 is a "whiskbroom style" instrument that collects data in a cross-track direction by mechanical scanning and in an along-track direction by movement of the airborne platform. The data were collected over the wavelength range from 437.9 nm to 2506.7 nm in 128 bands. The bandwidths at full width of half maximum (FWHM) varies from 13.3 nm to 22.3 nm with a spectral sampling interval range of 10.7 nm to 19.8 nm (Table 3). The aircraft was flown at an altitude of 2500 m resulting in a swath width of 2.5 km (512 pixels) and a

spatial resolution of 5 m. The Probe-1 sensor was mounted on an active 3-axis gyrostabilized real time motion compensation system. A non-differential GPS was recording the location of the aircraft during the flight but no attitude measurements were made.

Figure 3. Probe-1 Sensor Built By Integrated Spectronics For Earth Search Sciences Inc.

Table 3. Probe-1 Spectral Specifications

Detector Modules	Spectral Range	Spectral Bandwidth	Spectral Sampling Interval
Visible	437.9-904.3 nm	13.7-20.7nm	10.7-18.3 nm
N-IR	896.3-1355.3 nm	13.3-22.3 nm	12.5-19.8 nm
SWIR 1	1394.7-1801.1 nm	14.6-17.8 nm	11.7-15.6 nm
SWIR 2	1977.6-2506.7 nm	16.7-21.5 nm	13.9-18.9 nm

The airborne C-Band (5.66 cm) polarimetric SAR data were acquired by Environment Canada's CV-580, in narrow swath mode. Imagery was acquired on June 30th 1999 at incidence angles of 37° to 67°. The data were recorded in slant range and at a 4 m pixel spacing. For each radar pulse, 4096 samples of complex radar signal data are captured, providing 4096 pixels in the range direction. The system employs a real-time motion compensation system that relies on inputs from the inertial navigation system (INS) on board the aircraft (Hawkins *et al.*, 1999).

Black and white air photos (hard copy) covering the site were purchased. The photos were acquired in the first week of May 1999, at a scale of 1:15,000. As well, for each of the six fields, a digital orthophoto was purchased. In addition to the airborne data acquisitions, several satellite images were acquired. Six RADARSAT-1 Fine Mode acquisitions were planned (Table 4). As well, all available cloud free Landsat and SPOT imagery that covered the site during the growing season was ordered.

Table 4. Satellite Image Acquisitions

Satellite	Sensor / Modes	No. of Bands	Nominal Spatial Resolution (m)	Acquisition Date (1999)	Scene Centre Co-ordinate
RADARSAT-1	Fine 4 Far	1	8	June 2	43° 38' N; 81° 32' W
RADARSAT-1	Fine 4 Far	1	8	June 26	43° 39' N; 81° 34' W
RADARSAT-1	Fine 2 Far	1	8	July 3	43° 40' N; 81° 31' W
RADARSAT-1	Fine 4 Far	1	8	July 20	43° 39' N; 81° 31' W
RADARSAT-1	Fine 2 Far	1	8	July 27	43° 38' N; 81° 27' W
RADARSAT-1	Fine 4 Far	1	8	August 13	43° 41' N; 81° 34' W
SPOT-4	HRV2	4	20	July 7	43° 40' 28" N; 81° 25' 36" W
Landsat-7	TM	7	30	July 24	N/A

2.3 *Description of Ground Data Collection*

Ground measurements were collected from June 24 to July 7, 1999. Approximately ten sampling sites were selected per field to reflect within-field variability, based on elevation and soil maps (Figure 4). There were sixty sampling sites in total. All sites were marked with a flag and the location of the flag was recorded with a Differential GPS unit. Details of the numerous ground measurements collected during this field campaign are provided in the following sections.

Soil Moisture

On July 7th, soil moisture measurements were taken at each site, as well as within each bare soil patch, ± 2 hours of the SAR overpass. Moisture was determined by collecting soil samples using a 0-3 cm soil ring. Three replicate samples were taken within 1-2 metres of the centre of the site. Soil samples were weighed wet and then oven dried for 48-72 hours at 100°C, and then re-weighed. Volumetric 0-3 cm soil moisture was calculated using:

$$Soil\ moisture = \frac{(wet\ weight\ -\ dry\ weight)}{volume\ of\ cylinder} \qquad \textbf{(1)}$$

Soil Fertility

Both 2-inch and 6-inch soil samples were collected and analyzed for soil fertility. Only one fertility sample, at each depth, was collected at each site and in each bare patch. The 2-inch samples were collected from June 24 to July 7, 1999, using a specially designed shovel (Figure 5). Six-inch samples were collected using a soil core, on the day of the Probe-1 flight. Soil samples were analyzed for the following properties: nitrate nitrogen (N0$_3$_N), pH, organic matter (%), phosphorous (ppm), potassium (ppm), magnesium (ppm), calcium (ppm), zinc (ppm), manganese (ppm), texture (as a class), cation
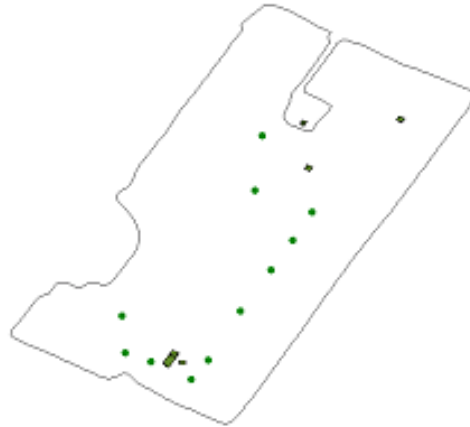
exchange capacity (MEW/100G), potassium saturation (%), magnesium saturation (%) and calcium saturation (%).

Figure 4. Location Of Sampling Sites And Patches Within Clinton '99 Fields
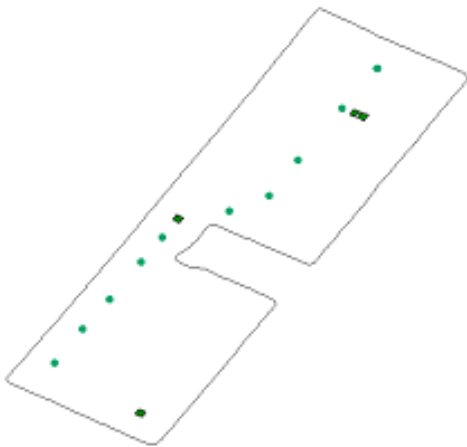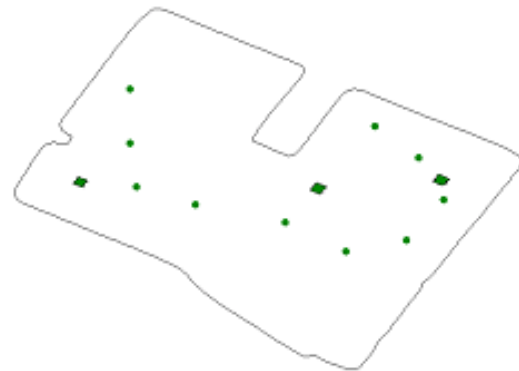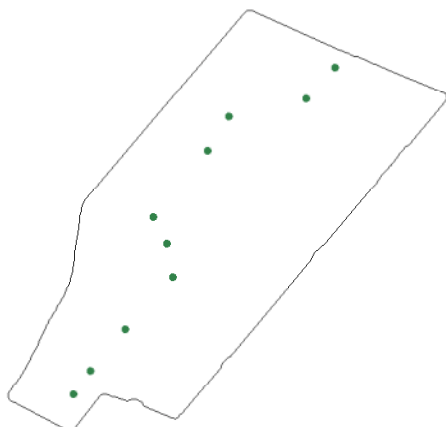
Forbes

Montgomery

Pig Barn

Sigma

Wright

Vanderyk

Figure 5. Custom Designed Shovel Used For 5 cm Soil Fertility Sample

Percent Ground Cover

Percent ground cover was calculated from vertical photographs taken with a 35 mm camera equipped with a 28 mm lens. The camera was mounted on an overhead mast at a height of 2 m above ground (Figure 6). In this configuration the camera viewed a ground area of 3.99 m^2. Since the Probe-1 data has a pixel size of 5 m by 5 m, photographs were taken 3 to 4 m surrounding the centre of the sample site locations. Three photographs were taken at each sampling site and in each patch. Photos were taken in the period from June 24 to July 7, 1999.

Figure 6. Ground Vertical Photograph Acquisition

SPAD Measurements

Simultaneous with the Probe-1 hyperspectral data acquisition, crop "greenness" was measured using the Minolta SPAD-502 meter (Figure 7). The SPAD-502 measures transmittance of plant leaves in the red and near-infrared spectral regions. The ratio of these two transmittances is proportional to the total leaf chlorophyll content (Boggs *et al.*, 1998). At each sampling site, 30 SPAD-502 measurements were collected on different plants in a 2 m area surrounding the centre of each sampling site. These measurements were taken on the plants upper most fully extended leaf. An average of the SPAD-502 measurements was then calculated for each sampling site. Measurements were collected on the day of the Probe-1 acquisition.

Figure 7. Minolta SPAD-502 Chlorophyll Meter

Leaf Area Index (LAI) Measurements

Ground LAI measurements were acquired using the LI-COR LAI-2000 (Figure 8). Measurements were taken in the period from June 24 to July 7, 1999. The instrument's algorithm measures effective LAI (eLAI) (LI-COR, 1990). It does not take into consideration the clumping index of the crop canopy. The clumping effect assumes that canopy foliage is spatially distributed according to a non-random pattern (Chen and Cilhar, 1995). Using this same data set, previous research reveals that eLAI values acquired with the LAI-2000 have a very good correlation (r = 0.90) with percent ground cover (Pacheco *et al.*, 2001a).

Three eLAI measurements were taken at each sampling site in order to minimise errors and thus, provide a representative eLAI average of the sample site. Measurements were acquired on 2 m transects along a diagonal between two plant rows within an area of 2 to 3 m surrounding the centre of the sampling site.

Figure 8. LI-COR LAI-2000 Instrument

The LAI-2000 measures the attenuation of diffuse sky radiation at five zenith angles (7°, 23°, 38°, 53° and 68°) simultaneously (LI-COR, 1990). At each sampling site, one reference measurement was taken above the crop canopy and four measurements were taken below. For each eLAI measurement, five canopy transmittance values are calculated from the five zenith angles of the optical sensor, which are utilized to calculate foliage amount and orientation.

Biomass Samples and Plant Water Content Estimation

To establish crop biomass and plant moisture levels, crop samples were gathered at all sites. At each site within the three bean fields, all above ground crop biomass within a standard 0.5 m x 0.5 m square was collected. Three replicate samples were collected at each site. These samples were immediately weighed to establish wet weight, and then as with the soil samples, oven dried and re-weighed. Gravimetric crop water content derived from these biomass samples was calculated by:

$$Plant\ Water\ Content\ =\ \frac{(wet\ weight\ -\ dry\ weight)}{wet\ weight} \qquad (2)$$

At each site within the corn fields, two corn plants were cut in each of two adjacent rows. Three replicate biomass samples were collected. For each replicate, the plants were weighed wet to establish total biomass. Because of the volume of plant biomass, each sample was subset. One corn plant per replicate was selected. This plant was weighed wet and then oven dried and re-weighed. The plant water content was then established for the sub-sample. With knowledge of the ratio of the weight of the total sample to the

15

weight of the sub-sample, total plant water content could be calculated for the entire sample. Biomass sampling occurred on the same day as the Probe-1 acquisition.
Plant Tissue Samples

At each site within the corn fields, tissue samples were gathered for lab chemical analysis. Samples were collected on the day of the Probe-1 flight. Enough upper corn leaves were collected to fill a small paper bag. Three replicates were taken at each site. These samples were then analyzed for the following properties: nitrogen, phosphorous, potassium, magnesium, calcium, zinc (ppm), manganese (ppm), copper (ppm), iron (ppm), boron (ppm).

Crop Height and Row Information

At the same time as the biomass and tissue sampling, crop height was also measured. At each site, the height of three plants was recorded. Once during the growing season, row direction was noted for each field. As well, row and plant spacing was recorded (five measurements per field).

GER-3700 Ground Spectra Measurements

A number of ground target spectral measurements were acquired during the field campaign. A GER3700 field spectroradiometer (Geophysical & Environmental Research Corp.) was used for all the measurements (Figure 9). When used with a reference white reflectance panel, this instrument can measure reflectance spectra of various surfaces over a large spectral range from 300 nm to 2500 nm with a large number of narrow spectral bands varying from 1.5 nm to 9.5 nm in width. The white reference panel used was a calibrated 10" x 10" white reflectance Spectralon panel. This panel reflects 98% to 99% of the sun's radiation equally over the spectral range covered by the GER3700.

Figure 9. GER3700 Field Spectroradiometer And White Reflectance Spectralon Panel

The purpose of these spectral measurements was to provide a spectral library of the main reflecting surfaces in the fields studied. Some of these reflecting surfaces were the two main crops (corn and white beans), the different soil types, the crop residue and the main types of weeds found in these fields. Another important use of the field spectroradiometer was to provide ground reference spectra of a large uniform surface to calibrate the Probe-1 airborne hyperspectral sensor. Unfortunately, due to the frequent presence of clouds during the field campaign, the number of spectral measurements planned was never reached. Table 5 summarizes the dates and number of spectra acquired in three of the fields.

Table 5. Description Of Field Spectra Acquisitions

Field Name	Crop Type	Date	Number of Spectra
Montgomery	White Beans	June 26	39
		July 5	103
Pig Barn	Corn	July 2	49
Forbes	Corn	July 4	56

Yield Maps

Cargill and AFL provided 1999 yield maps (Figure 10) for two of the corn fields (Forbes and Wright), as well as for the three bean fields: Montgomery, Sigma and Vanderyk. The two wheat fields were harvested on July 14th, and yield maps for these two fields were provided by AFL. Yield for Montgomery and Sigma were recorded as 'normalized yield'. Normalized values were provided since two combines were used during harvest and the two yield files were integrated together. Due to calibration differences on the combines, the yield was normalized. The scale of the yield maps is in percent above and below the average of the field. Average yield for Montgomery was 37.4 BPA. Therefore 100% in the normalized yield equates to the average of the field. The remaining percentages are below and above the average yield for the field (i.e. 80% of the average is actually 20% lower than the average of the field, and 150% means 50% higher than the average). Average yield for Sigma was 30.7 BPA.

List of Ancillary Data Collected

In order to help the planning of the field campaign and the location of sampling sites and "pure" patches in these fields, topography and Electro-Magnetic Induction (EMI) survey data were provided by AFL. Before the beginning of the field campaign, Cargill provided a series of agricultural scout reports describing the health status of the crop and the presence of weeds in each of these fields. Cargill also provided reports from a special series of scout visits that were based on an image of each field acquired by the Probe-1 on

July 7. These post-acquisition scout reports were used to interpret the fraction map products generated from the Probe-1 imagery.
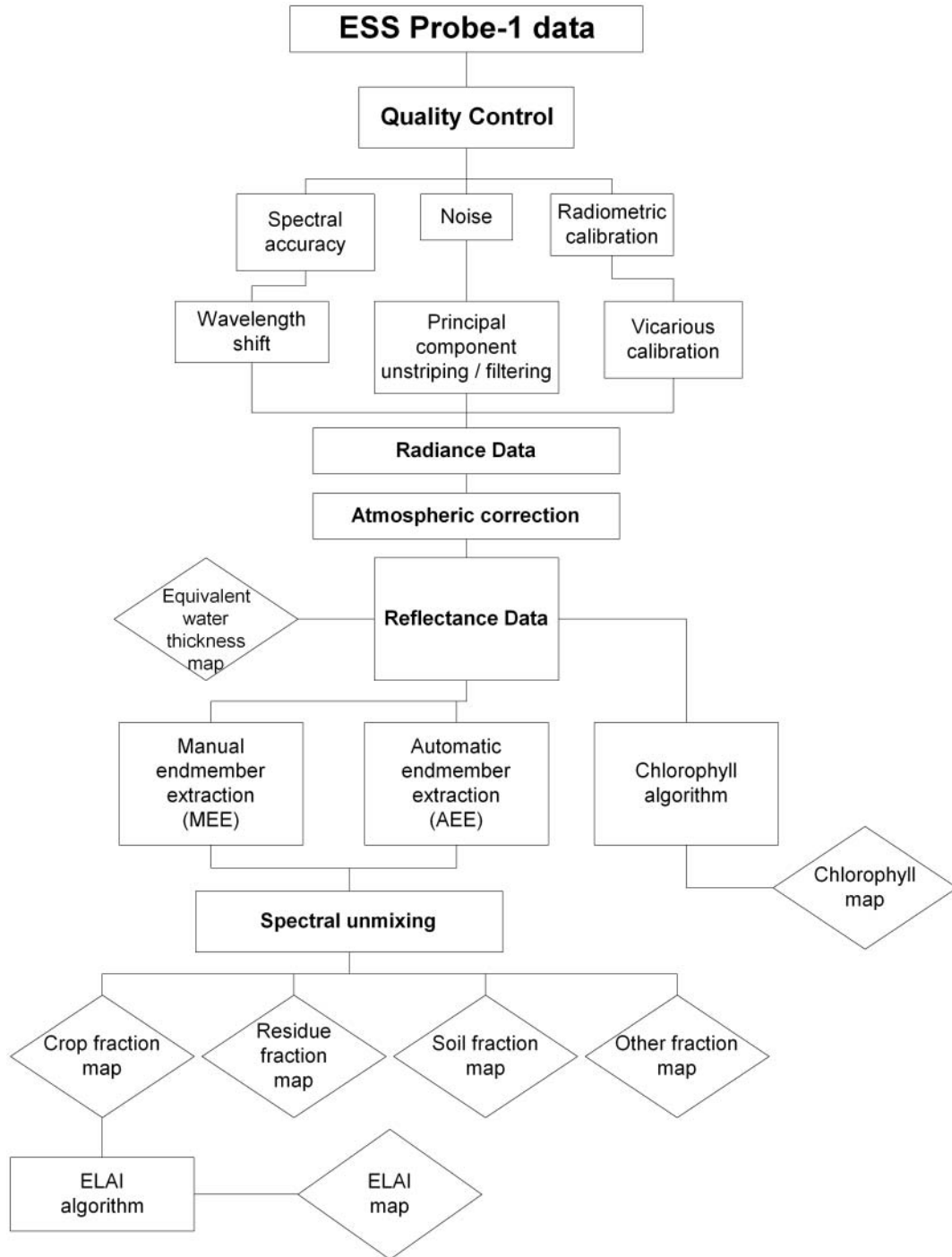
Figure 10. Yield Maps Of The Clinton '99 Fields Provided By Cargill And AFL
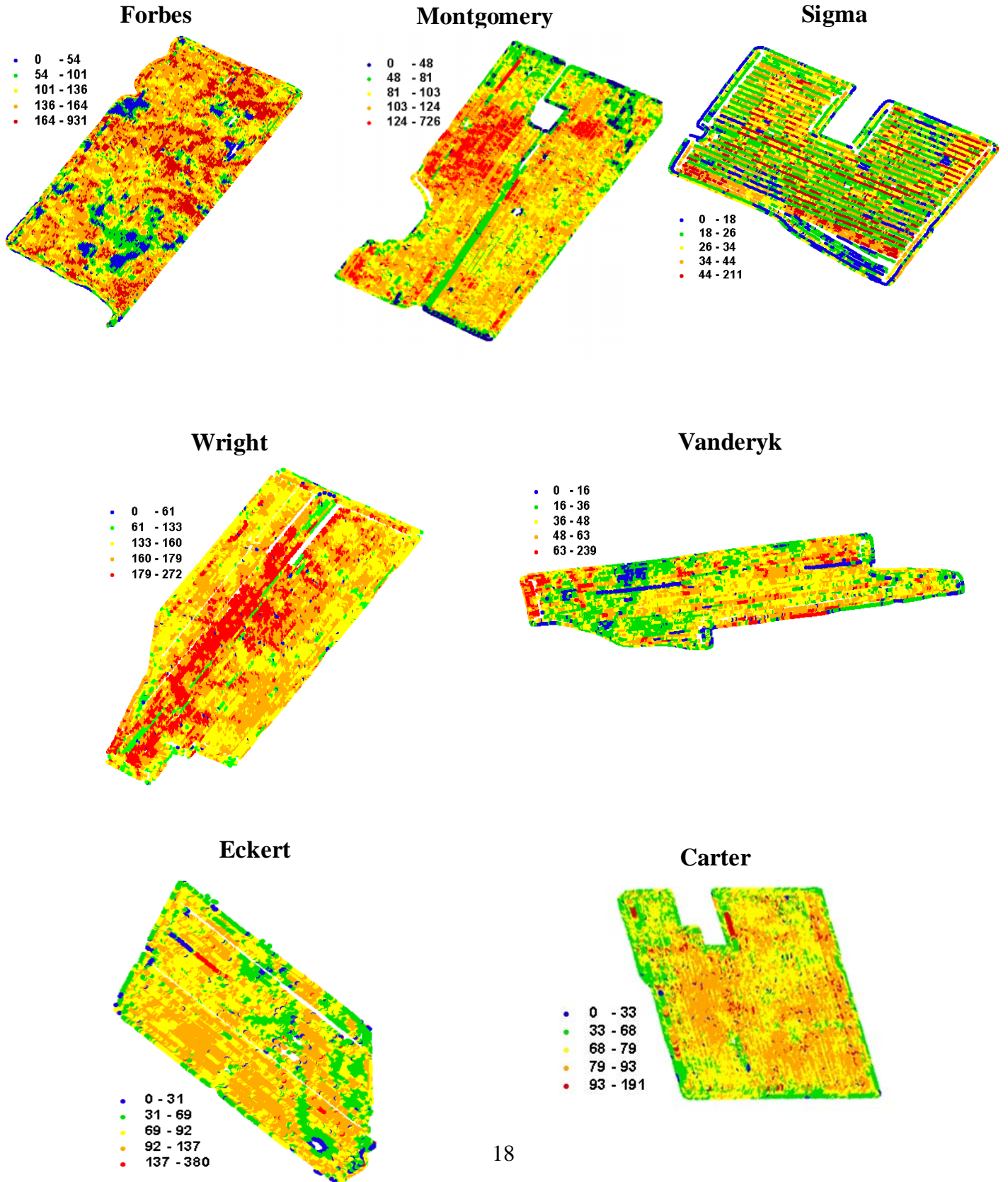
3. Data Processing Steps

The flow chart presented in figure 11 identifies the data processing steps and data product outputs for the Clinton Probe-1.

Figure 11. Probe-1 Data Processing Steps And Product Outputs

3.1 *Ground Spectral Reflectance Calibration*

The original reflectance measurements acquired with the GER3700 field spectroradiometer were first adjusted for the spectral and geometric response of the white Spectralon reference panel. These adjustments were based on panel calibration factors measured in a spectroradiometric laboratory and applied using a CCRS in-house program.

3.2 *Probe-1 Calibration and Atmospheric Correction*

Image pre-processing and information extraction was carried out using the Imaging Spectrometer Data Analysis System (ISDAS) (Staenz *et al.*, 1998). The Probe-1 data were converted to at-sensor radiance using a vicarious calibration approach (Secker *et al.*, 2001). In order to use this method, reflectance spectra were acquired using a GER3700 field spectroradiometer. These reflectance spectra were measured within the central bare soil patch in Montgomery. This method was used to generate a new set of calibrated gains to convert the raw digital numbers (DN) from Probe-1 to radiance. The MODTRAN3 radiative transfer code, implemented within ISDAS using a look-up table (LUT) approach (Staenz and Willams, 1997), was then used to correct the Probe-1 radiance spectra to surface reflectance.[2]

3.3 *SAR Processing and Calibration*

Corner reflectors and PARCs (Polarimetric Active Radar Calibrators) were deployed just north of Wingham (Ontario) during the airborne SAR acquisitions (Figure 12). Data from these instruments were used for radiometric calibration of the airborne data. Polarimetric processing and radiometric calibration of the airborne data was accomplished using the CCRS programs POLGASP and COMPLEXCAL. Within scene calibration accuracies were less than 1 dB.

Image products were synthesized from the complex data using the CCRS software package POLSIG. Four linear transmit-receive polarizations (HH, VV, HV, VH), as well as the three circular polarizations (RR, RL, LL) were generated. In addition, co-polarization plots and the co-polarized phase difference images were created.

3.4 *Registration of Site Locations to Probe-1 Imagery*

To preserve the spectral integrity of each pixel in the imagery, no geometric correction of the Probe-1 data was attempted. To locate the Probe-1 pixels where ground sampling was done in each field, a reversed image-to-image registration process was used. All sampling site locations were accurately measured with a differential GPS during the field campaign. The positions of these sites were marked on the digital aerial orthophotos. These marked orthophotos were then registered by a polynomial fit to the Probe-1 imagery until the boundaries of each field used in this study fit the boundaries of the same field in the original Probe-1 imagery. The pixel-line locations of the sampling site

20

markers in the Probe-1 imagery were located by this reverse process and used for the correlations between the hyperspectral data products and the ground measurements.

Figure 12. Corner Reflectors Deployed During The Airborne SAR Acquisitions

3.5 *Description of Methods to Extract Information From the Probe-1 Imagery*

Several conference papers have been presented on the Clinton '99 analysis and results (McNairn *et al.*, 2001a; McNairn *et al.*, 2001b; Pacheco *et al.*, 2001a; Pacheco *et al.*, 2001b). The validations of both the LAI and EWT algorithms are the subject of two M.S. theses at the University of Ottawa.

Spectral Unmixing

Reflectance recorded for each pixel within an image is a combination of the reflectances from all "contributors" or "endmembers" in that pixel. In an agricultural context, these endmembers are likely to be crop and soil, along with other contributors such as weeds, crop residue and shadow. The purpose of spectral unmixing is to determine the relative contribution of each of these endmembers to the total reflectance recorded for each pixel. The output of spectral unmixing is a series of fraction maps which indicate the proportion (0 to 1) of each endmember (crop, soil, weed, residue, shadow) present in each pixel.

Using the Probe-1 data, constrained linear spectral unmixing was performed using an algorithm implemented in ISDAS (Staenz *et al.*, 1998). Two different methods were explored for the extraction of endmember spectra. The first method used an algorithm

implemented in ISDAS called Automatic Endmember Extraction (AEE) and the second method was a manual endmember extraction (MEE) approach. Results from both methods will be discussed in this report.

Endmember spectra were manually extracted from the image data (MEE approach) based on knowledge of the fields. Since the availability of pure pixels under natural field conditions is problematic, patches of crop residue and bare soil were artificially created in the primary fields. Endmember spectra were extracted from the canopy within these 20 m by 20 m patches. The patches did not exist in all investigated fields and some endmember spectra from one field were used on the other two fields of the same crop type. Double crop density patches were not "pure" but did consist of about 80% crop and the residue patch did contain a small amount of green grass. However, soil patches were 100% soil. Spectral unmixing was done using the spectral range from 430 nm to 2500 nm. Spectral unmixing of the hyperspectral Probe-1 data using the MEE approach was conducted with three endmembers: vegetation (crop), soil and residue. Fraction maps of these endmembers were then derived. The spectral unmixing process described above was completed on both the radiance and the reflectance data sets.

The fraction maps were validated with the vertical photographs taken during the field campaign. The vertical photographs were digitized in three channels (blue, green and red). Unsupervised classification was carried out using ten classes: three classes for soil, three classes for leaf cover, two for residue, one for soil shadow, and one for leaf shadow. These classes were then aggregated to form three major components: leaf cover, residue, and soil. Once the classification was completed, percentages of leaf, soil and residue cover were determined for each photograph. For each of these classes, percent ground cover was then calculated from the average of the three replicate photographs. These percent cover classes were used to validate the crop, soil and residue fraction maps created by spectral unmixing.

Canopy Liquid Water Content

Canopy liquid water content can be estimated from the liquid water absorption features at 970 nm and 1180 nm. Within ISDAS, this is computed as the Equivalent Water Thickness (EWT). EWT is the thickness of a hypothetical layer of water in the crop canopy that is required to produce the equivalent absorption feature observed in the hyperspectral data. EWT is estimated from the Probe-1 imagery using an iterative curve fitting approach. This approach combines atmospheric correction and non-linear least squares regression modelling for parameter estimation (Staenz *et al.*, 1997).

The depth of the water absorption feature is related to the overlapping absorption of atmospheric water vapour and plant liquid water. The absorption peak of liquid water is offset to longer wavelengths by approximately 20 nm. Thus the minima of each absorption feature are offset and these two absorption effects can be separated. A non-linear least squares curve-fitting technique (Gao and Goetz, 1990) and a radiative transfer code are used to estimate column atmospheric water vapour and to separate atmospheric water vapour from canopy liquid water.

The model retrieves both the atmospheric water vapour content and the canopy liquid water on a pixel-by pixel-basis. Maps of EWT were produced for each of the fields under study.

Leaf Area Index

Maps estimating effective Leaf Area Index (eLAI) were also generated from the Probe-1 hyperspectral data. eLAI is estimated using the crop fraction maps derived from spectral unmixing. Unlike other methods, this approach means that only the crop portion of vegetation (excluding weeds or volunteer crops) is taken into account when estimating LAI. eLAI values were extracted from the hyperspectral data using an algorithm implemented in ISDAS (Staenz *et al.*, 2001). The crop fraction for each of the fields was used as input to produce the eLAI map.

eLAI can be calculated according to this formula (Ross, 1981):

$$eLAI = \frac{\cos \alpha}{G} \left(- \ln P\right) \qquad \qquad \textbf{(3)}$$

where P is the probability of a view line or a beam of radiation at an incidence angle α passing through a horizontally uniform plant canopy with random leaf angular and spatial distribution and G is the mean projection coefficient of unit foliage area on a plane perpendicular to α.

To estimate eLAI from hyperspectral data, G (α) can be determined at 0.5 for plants which have randomly distributed leaf angles such as agricultural crops (Norman, 1979). The incidence angle α corresponds to the sensor viewing zenith angle. Probe-1 is usually flown at a view angle of 0° (nadir looking). Also, P represents the gap (non-vegetation) fraction, which is determined by spectral unmixing as follows:

$$P = 1 - fc \qquad \qquad \textbf{(4)}$$

where fc is the fraction of the crop endmember. eLAI is then derived from hyperspectral data according to the following formula:

$$eLAI \ (fc) \ = \ -2 \ln \ (1 - fc) \qquad \qquad \textbf{(5)}$$

Chlorophyll Content

Chlorophyll maps were generated for each field using Probe-1 reflectance data. Three methods were selected from the literature based on their potential for the calculation of chlorophyll maps from hyperspectral data. These three methods generate separate estimates for chlorophyll *a*, *b* and major carotenoid pigments. Since SPAD-502 field measurements are related to the total chlorophyll content of the plants and since chlorophyll *a* at this stage of plant growth is usually the major contributor to total

chlorophyll variability, only chlorophyll *a* and related indice (PSSR$_a$, PSND$_a$) estimates will be reported.

The first method is proposed by Chapelle *et al.* (1992) and called the Ratio Analysis of Reflectance Spectra (RARS). In this approach, absorptions in the reflectance spectra due to plant chlorophyll content are enhanced using a ratio analysis. A ratio image is calculated from the original reflectance spectra through two steps. First, the reflectance spectrum recorded for each pixel is divided by the reflectance spectrum of a chosen reference area. The reference spectra are taken directly from an area of the imagery assumed to have maximum chlorophyll content for this crop. Then, the ratio image is calculated from the standardized image by dividing the reflectance at 675 nm by the reflectance at 700 nm, which Chappelle *et al.* (1992) demonstrate has a strong linear relationship to the chlorophyll concentration. The slope and intercept of the model are derived by regressing chlorophyll measured in the lab with the reflectance ratio. Since chlorophyll data were not collected, the coefficients used for this analysis were defaulted to those given in Chappelle *et al.* (1992). Based on this methodology, maps of crop chlorophyll were generated.

The other methods are based on two chlorophyll indices called the Pigment Specific Simple Ratio (PSSR$_a$) and the Pigment Specific Normalized Difference (PSND$_a$) (Blackburn, 1998). The PSSR$_a$ is a simple ratio of reflectance at two optimal wavelengths, in this case 810.4 nm and 676.0 nm for chlorophyll *a*.

$$PSSR_a = R_{810.4} / R_{676.0} \qquad\qquad \textbf{(6)}$$

PSND$_a$ is a type of normalized index using the same optimal wavelength as PSSR$_a$ for chlorophyll *a*.

$$PSND_a = (R_{810.4} - R_{676.0}) / (R_{810.4} + R_{676.0}) \qquad\qquad \textbf{(7)}$$

3.6 *Statistical Analysis of the Hyperspectral Image Products*

Crop fractions were correlated with the percentage crop cover estimated from the classified photographs. The chlorophyll content maps were compared with SPAD-502 measurements. Values of eLAI generated from the crop fraction maps were correlated with measurements taken with the LAI-2000. To compensate for the uncertainty in the location of the ground sampling sites in the Probe-1 imagery fraction, chlorophyll and eLAI values were averaged on a 3 by 3 pixel window surrounding the location of the sample site in the imagery. Correlations were run on data pooled from all bean and corn sites. The number of sample sites within a field (8 to 11) was generally not sufficient to run regression analysis on a field-by-field basis.

3.7 *SAR Data Analysis*

Linear polarization composites (HH, VV, HV) were created for each of the corn and white bean fields. The radar response over these fields was assessed qualitatively. Yield data were acquired over two wheat fields in the study site and the sensitivity of backscatter to areas of high and low productivity on these wheat fields was assessed quantitatively. Unfortunately, wheat and barley were not chosen for study during the experimental design and thus, no within-field sampling of any small grain crops occurred. As a result, analysis focused only on correlations between the yield data and the SAR backscatter. Backscatter values were extracted from areas of high and low yield (as indicated by the yield monitor data) within each field. The three linear polarizations were then used to classify each field into regions of low and high backscatter. Yield monitor data were segmented into two regions as well – higher and lower yielding areas. The percent agreement between these two regions was then calculated.

4. Results and Discussion

4.1 *Spectral Unmixing*

Fraction Maps Derived From Automatic Endmember Extraction (AEE)

A critical element for spectral unmixing methods to generate meaningful results is the identification and choice of representative "pure" endmembers. The more the spectras are representative of these endmembers, the more accurate the quantitative map of each of these reflectors in a scene will be. In other hyperspectral applications, these endmember spectra can be obtained from existing spectral libraries. Unfortunately for agricultural applications, the large spectral variability of vegetation due to growing conditions (i.e. water, nutrients, solar radiation, infestations), growth stages and crop varieties impend the use of such libraries at this time.

A method to extract automatically "pure" endmembers from hyperspectral imagery has been developed at CCRS and implemented in ISDAS. Although the AEE method has produced interesting results for other hyperspectral applications, interpretation of the results was difficult when used with the data acquired for this project.

The AEE algorithm was run within ISDAS generating a set of endmember spectra. These spectra were then plotted and used in the spectral unmixing module of ISDAS to produce a fraction map for each of the selected endmembers. These maps showed the contribution of each endmember to the total reflectance of each pixel. Finally, with the help of the plotted endmember spectra, fraction maps were compared to the scouting reports that were completed after the hyperspectral overflight (Figure 13).

Figure 13. Fraction Maps Derived Using The AEE Approach

a) Sigma

High Vigor Crop
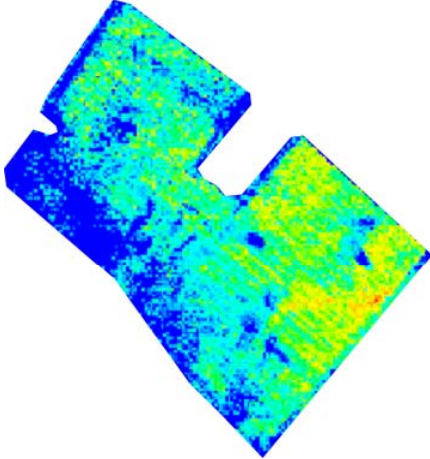
Low Vigor Crop
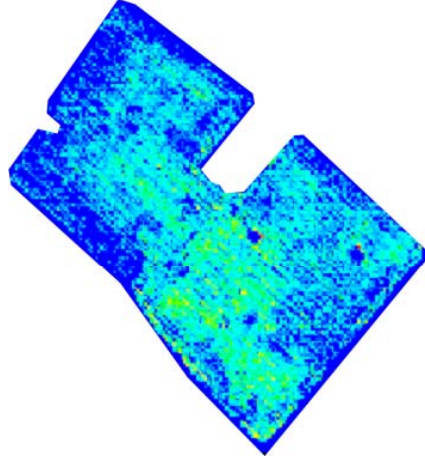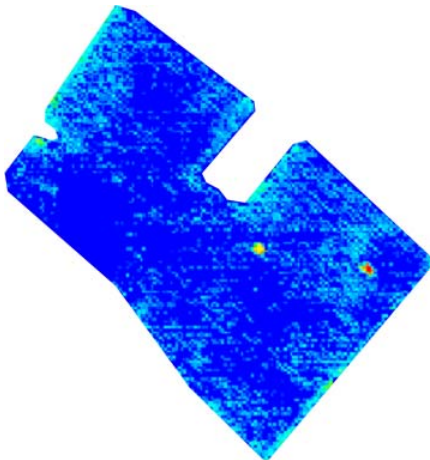
Soil

Soil
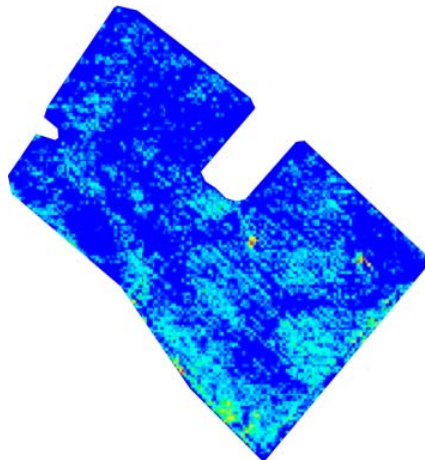
Soil
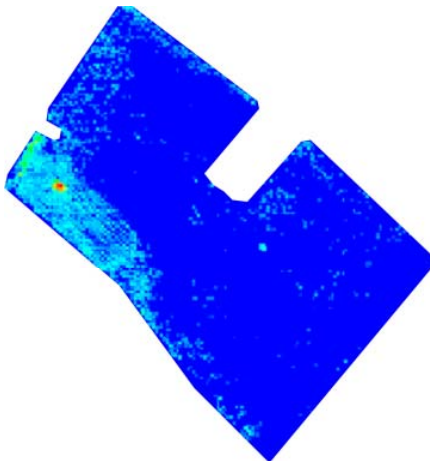
Drier Soil Areas
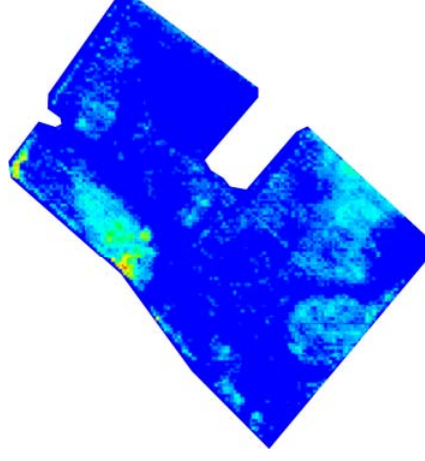
Root Rot Areas
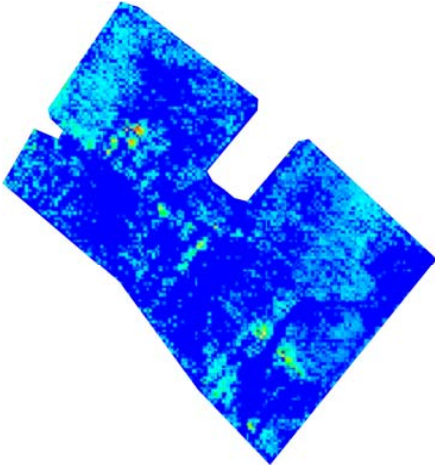
Around Root Rot Areas
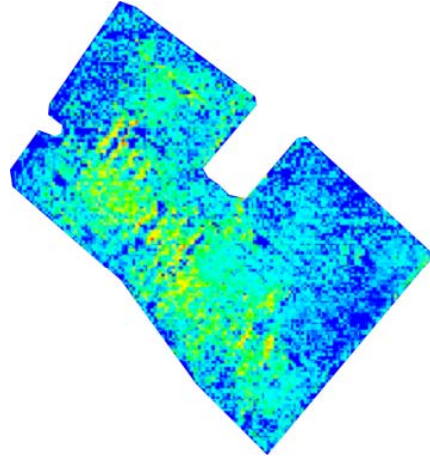
Around Root Rot Areas

Weedy Areas

Color Bar:

0   1
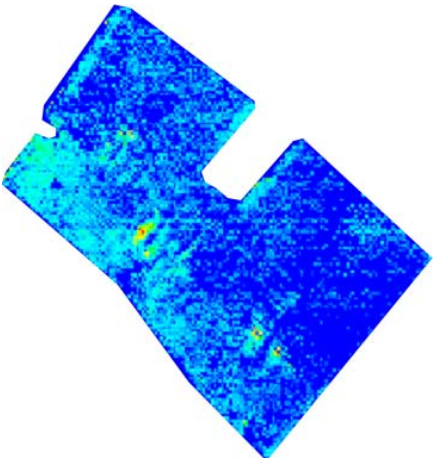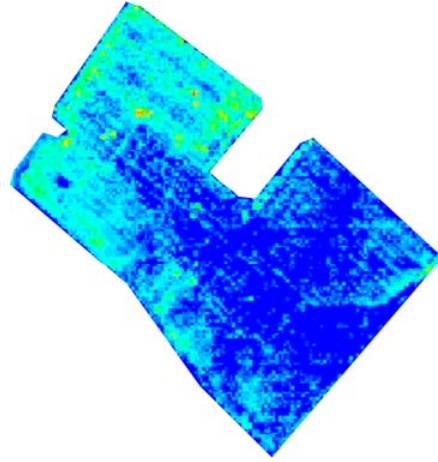
b) Montgomery

High Vigor Crop
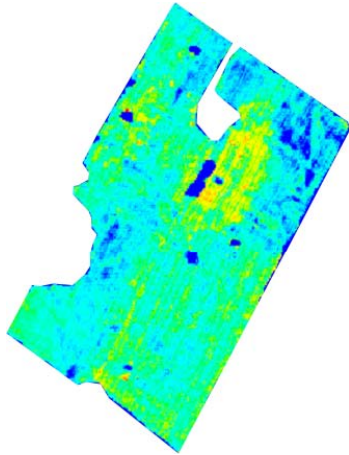
Low Vigor Crop
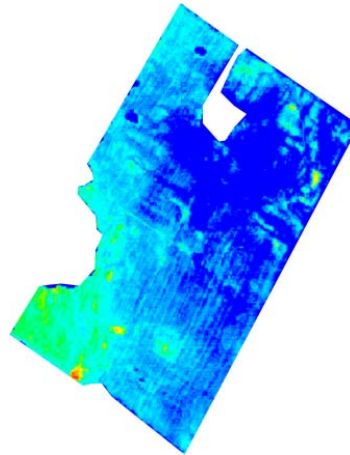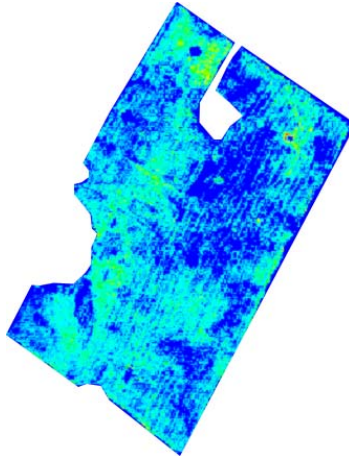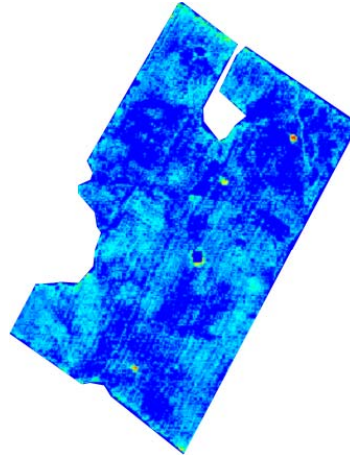
Low Vigor Crop

Soil

Drier Soil Areas
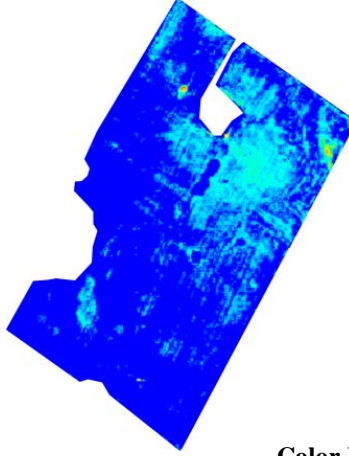
Around Root Rot Areas

Color Bar:

0   1
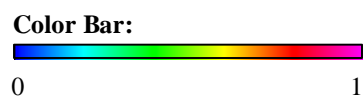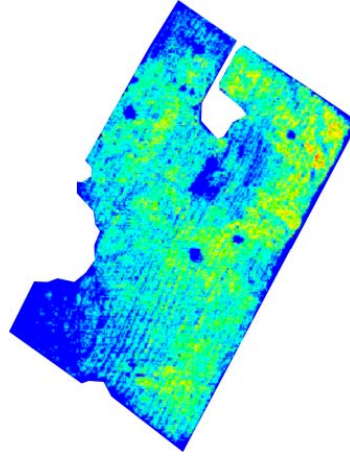
c) Forbes

High Vigor Crop
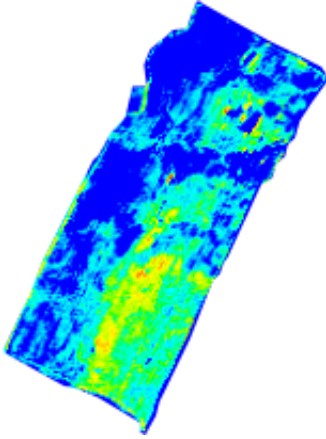
Low Vigor Crop
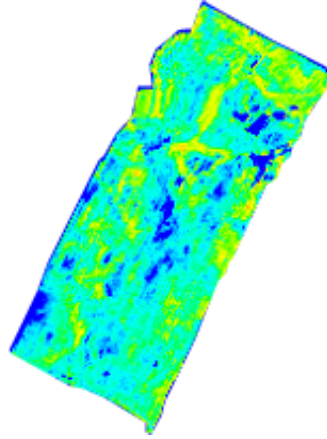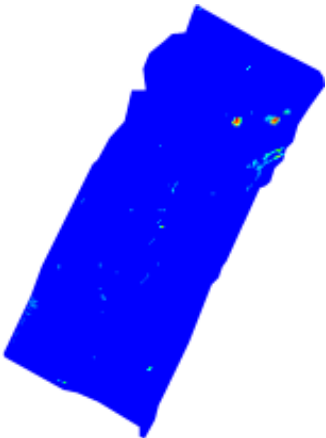
Soil

Moist Soil Areas
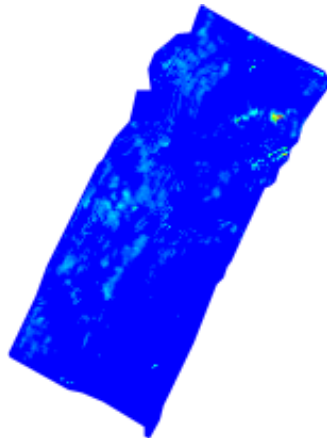
Darker Soil Areas
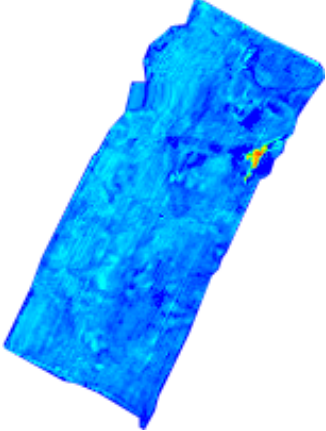
Darkest Soil Areas

Weedy Areas

Color Bar:

0   1
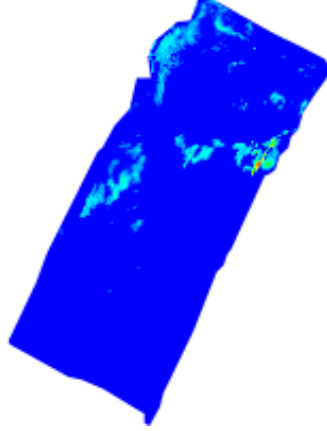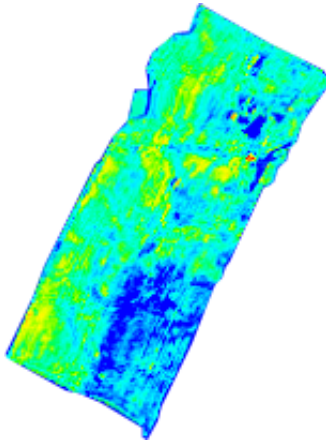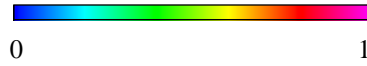
d) Wright

Highest Vigor Crop
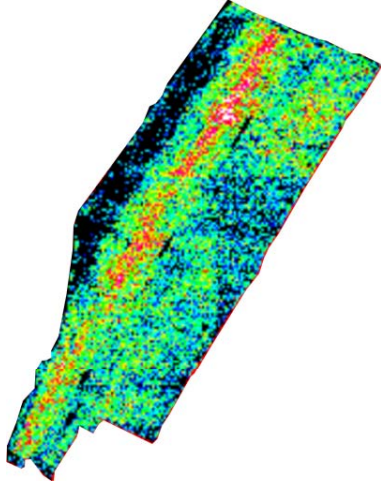
High Vigor Crop
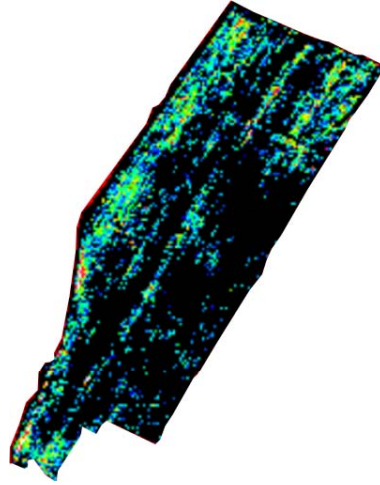
Moderate Vigor Crop
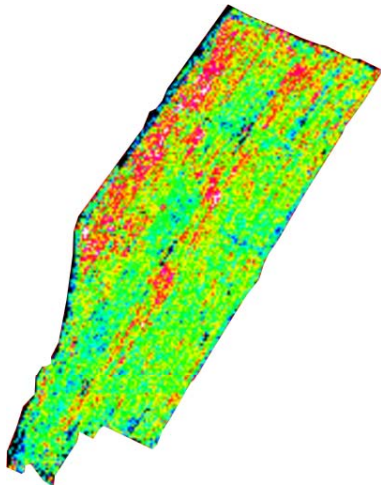
Moderate Vigor Crop
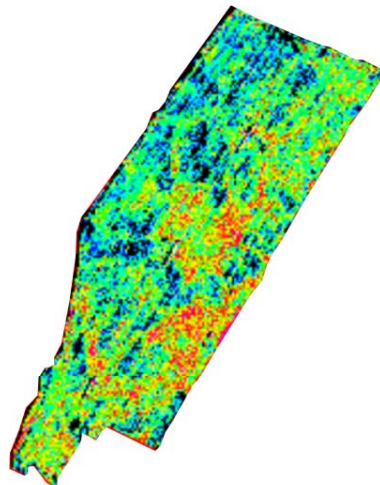
Low Vigor Crop
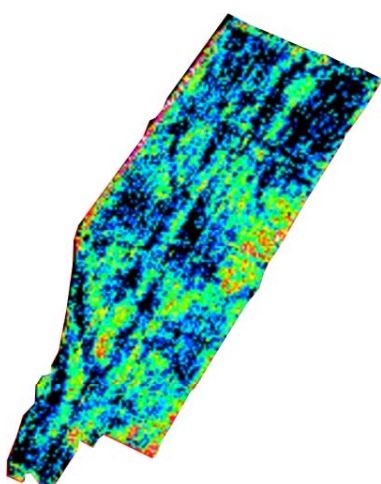
Low Vigor Crop/Soil Influence

Soil

Color Bar:

0   1
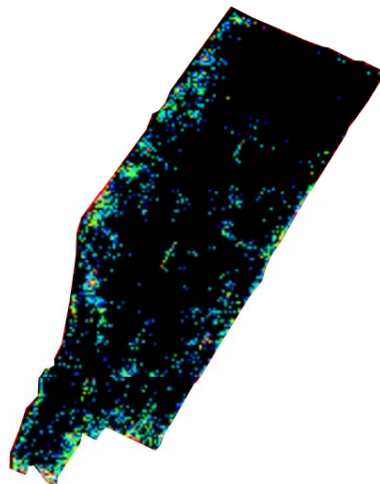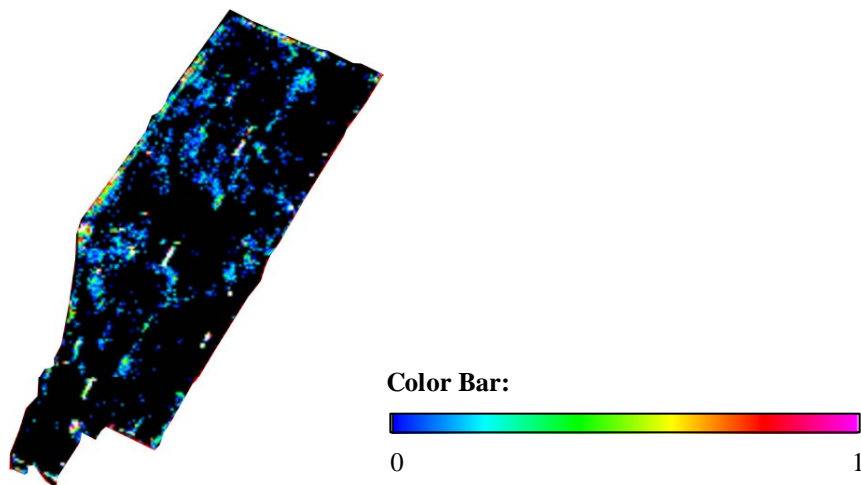
The AEE approach was first used on the entire scene of hyperspectral imagery including many of the surrounding farms, road and structures. The AEE algorithm selects the endmembers in the scene as a function of their level of spectral "purity" and not by the level of significance for the application. As a result the system selected many irrelevant reflecting surfaces as endmembers (roof barns, asphalt roads, etc.). To eliminate some insignificant endmembers, the automatic search for endmembers was then limited to a Region of Interest (ROI) just covering the fields used in this study. Targets known to be spectrally distinctive from their surroundings and uniform over many pixels (e.g. large blue plastic tarps), were easily identified as endmembers by this automatic method. Bare soil patches and field residue patches artificially prepared for this experiment were also recognized as endmembers.

One parameter that can be adjusted in the AEE algorithm is the number of endmembers requested by the user. Too many endmembers confused the interpretation but without enough endmembers, significant endmembers can be missed. Thus it was difficult to determine the optimal number of endmembers. By trial and error, the choice of fifteen endmembers appeared to be a good compromise. Of these initial fifteen endmembers, some could be immediately eliminated based on their spectral signature. Some of these rejected endmembers showed peaks and troughs caused by errors in the atmospheric correction at these pixels. The remaining endmembers were then compared to known features of the fields such as those reported by the crop scouts.

Except for Montgomery, the AEE method seemed to have difficulty distinguishing residue from stressed vegetation. With fraction maps obtained from constrained spectral unmixing, the algorithm forces the sum of all endmember fractions to equal 1. If some endmembers are not spectrally pure, the algorithm will try to calculate the best contribution of these endmembers. This "constraining" rule influences the quantitative estimate of all the endmembers.

Based on a qualitative assessment, some of the fraction maps produced from the AEE corresponded well to areas of stressed vegetation delineated on the scouting reports (Figure 14). Certain fraction maps based on the AEE approach corresponded to weed areas. The automatic selection of endmembers seems able to distinguish subtle differences between vegetation types (i.e. trees, different crops, weeds) but this distinction is not consistent.

The main disadvantage of the AEE method for agriculture is the difficulty in identifying or labeling the endmembers. The identification of these endmembers requires detailed knowledge of the fields at the time of the hyperspectral acquisition. Further investigation is needed to establish decision rules regarding the selection of the number of endmembers and in the interpretation of these endmembers.

Fraction Maps Derived From Manual Endmember Extraction (MEE)

An alternative approach to AEE is to extract spectra of "assumed" pure endmembers directly from the hyperspectral imagery. In this campaign, Cargill prepared special "pure pixel" patches prior to the hyperspectral acquisition (described in section 2.1). This approach is described as the Manual Endmember Extraction (MEE) method. Using this method, only three endmembers were selected – crop, soil and residue. These are the three dominant classes of reflectors found in these agricultural fields.

The crop, soil and residue fractions of each pixel were derived using the endmembers extracted manually from the Probe-1 images and a constrained linear unmixing method (Figure 13). The crop fractions were correlated with the percent crop cover calculated from the vertical ground photographs. Data from all fields were pooled for this analysis (n = 48). A correlation coefficient (r-value) of 0.850 was achieved when the crop fractions derived from unmixing of the radiance data were regressed against percent crop cover derived from the photographs. In comparison, a coefficient of 0.883 was achieved when the reflectance data were used.

These correlation results indicate that spectral unmixing is able to provide information on the extent of crop ground cover. Although correlations are significant, it is clear that some variability is still unexplained. Spectral reflectance from 3-dimensional targets like crop canopies is also dependent upon characteristics of the volume. Thus in future analysis several crop measurements should be combined into a more robust representation of the crop canopy. The unexplained variance could also be related to limitations in the endmember selection, and this requires further investigation. Endmembers were selected from patches of crop that were not "pure" endmembers since crop cover was not complete. In addition, endmembers were extracted from one field, but were used for unmixing on other fields.
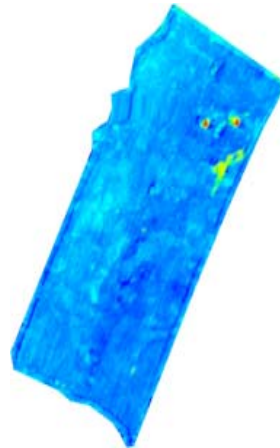
Figure 14. Fraction Maps (Crop, Soil And Residue) Derived Using The MEE Approach
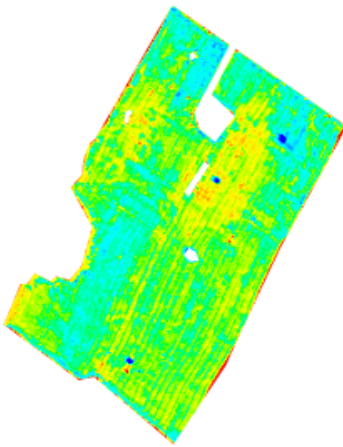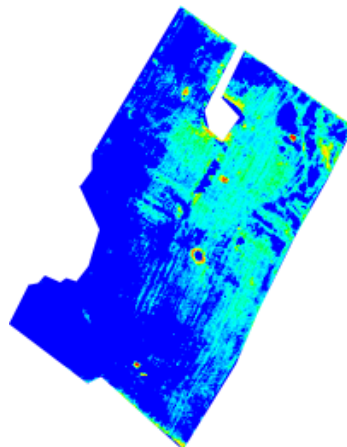
Forbes
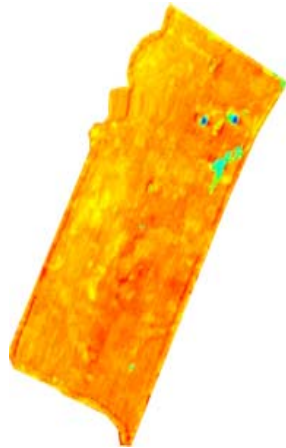
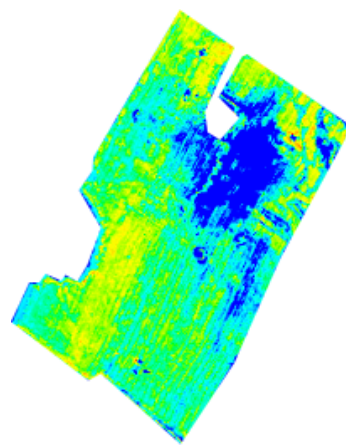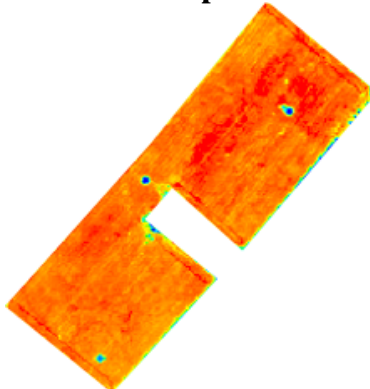Crop Fraction   Soil Fraction
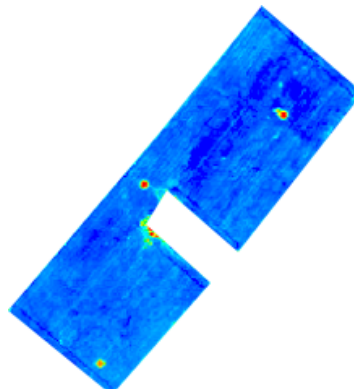
Montgomery

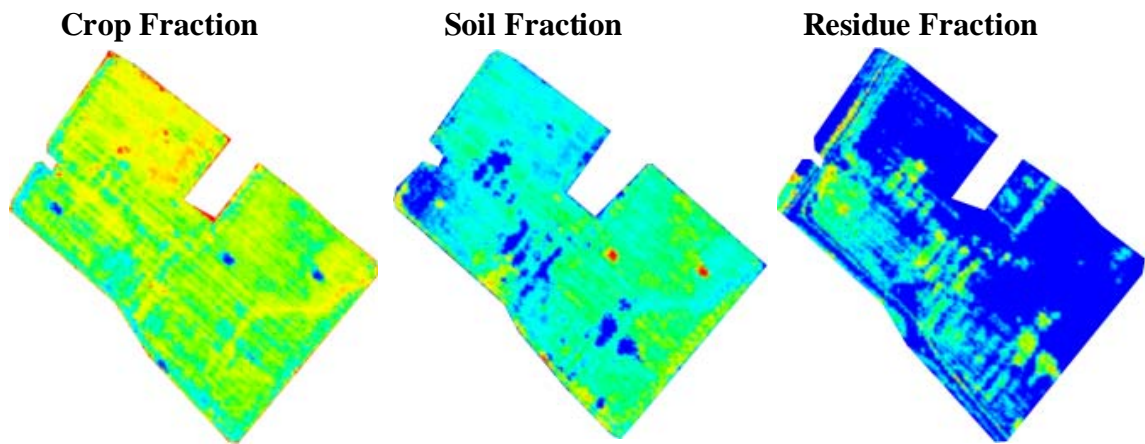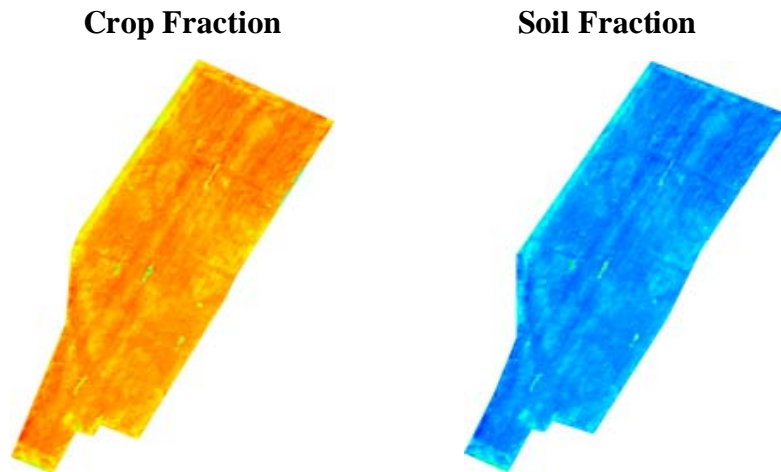Crop Fraction   Soil Fraction   Residue Fraction

PigBarn

Crop Fraction   Soil Fraction

Sigma

Crop Fraction　　　**Soil Fraction**　　　**Residue Fraction**

Wright

Crop Fraction　　　　　**Soil Fraction**

Vanderyk

Crop Fraction　　　　　**Soil Fraction**

Color
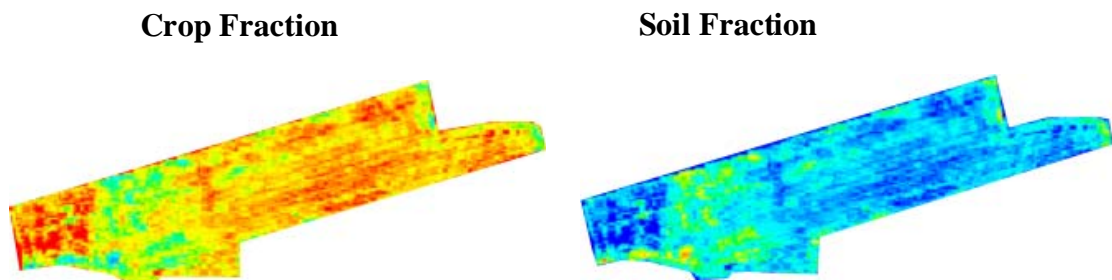
0　　　　　　　　　　　1

Correlation coefficients (0.850 compared to 0.883) were very similar regardless of whether the fraction maps were derived from reflectance data or from radiance data (Figures 15 and 16). This observation suggests that for this particular application, atmospheric correction of hyperspectral data may not be required. For operational near-real time crop monitoring, the elimination of this preprocessing step would be a very significant advantage.

The main disadvantage of the MEE method for agriculture is the difficulty in identifying pure pixels in the imagery. For the purpose of this experiment, pure endmember pixels were artificially created. A solution to pure pixel selection will have to be investigated for operational application.

Figure 15. Correlation Between Crop Fractions Derived From Probe-1 Radiance Data And Percent Crop Cover
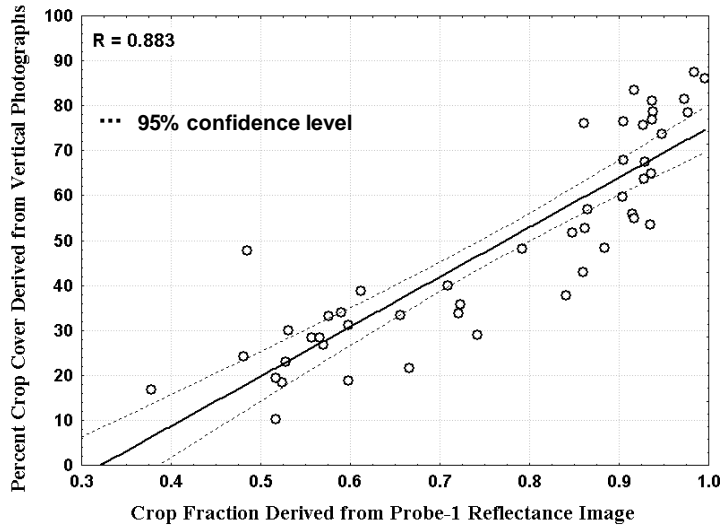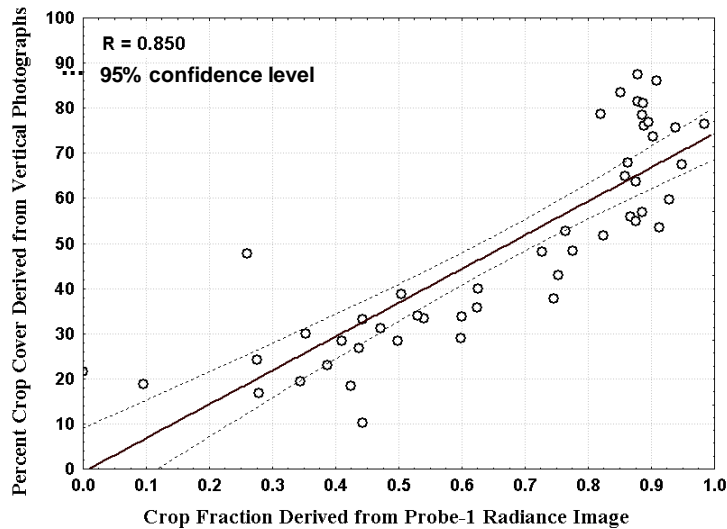

Figure 16. Correlation Between Crop Fractions Derived From Probe-1 Reflectance Data And Percent Crop Cover

4.2 *Chlorophyll Estimation*

Sample numbers were too small to run correlations between SPAD-502 measurements and chlorophyll estimates on a field-by-field basis. In some cases, as few as eight sample points per field were available. Within one crop type (beans or corn), correlations were weak (r-values less than 0.6) or were non-significant. These poor results are a reflection of the low variability in chlorophyll among sites within one crop type. Although sampling sites were chosen to maximize variability and crop cover did vary among these sites, SPAD-502 values were very similar as reflected in the low standard deviations (Table 6). Thus with only one acquisition date, variability in chlorophyll within one crop class is very limited and is not detected by either the SPAD-502 or the hyperspectral imagery (Figure 17).

Table 6. Comparison Between Chlorophyll Estimates Derived From Probe-1 And SPAD-502 Measurements

	White Beans		Corn		*Difference between means*
	Mean	*Std. Dev.*	**Mean**	*Std. Dev.*	*(corn - white beans)*
SPAD	**42.18**	*1.66*	**58.37**	*2.79*	*16.19*
RARS	**9.85**	*0.78*	**11.86**	*0.54*	*2.01*
PSNDa	**0.49**	*0.05*	**0.75**	*0.13*	*0.26*
PSSRa	**3.04**	*0.46*	**10.23**	*1.11*	*7.19*

Chlorophyll estimates from the Probe-1 imagery were then averaged for each crop type and compared to the average SPAD-502 measurements. These statistics are given in Table 6. On average, SPAD-502 values were higher for the corn crops, and this increase is also observed in the chlorophyll estimates from the Probe-1 imagery. The difference between the chlorophyll estimates for corn and beans was greatest for the $PSSR_a$ chlorophyll index. The greater sensitivity of this index supports the conclusions presented by Blackburn (1998) that this method seems the most appropriate to estimate plant chlorophyll *a* content per unit area at the canopy level.

The sensitivity of the Probe-1 derived products to differences in chlorophyll between the corn and bean crops indicates that this approach will likely work if variability exists. However these approaches need to be tested on a multi-temporal data set, where greater variability is probable, or in a field campaign where chlorophyll variability is induced. To improve chlorophyll estimates from hyperspectral data, bands should be narrower and be centered on the chlorophyll absorption features. The sensitivity of these chlorophyll estimation methods to band characteristics should be investigated.

4.3 *eLAI Estimation*

Results from the correlations between ground eLAI measurements using the LAI-2000 and eLAI values derived from the hyperspectral data cubes are presented in Table 7.

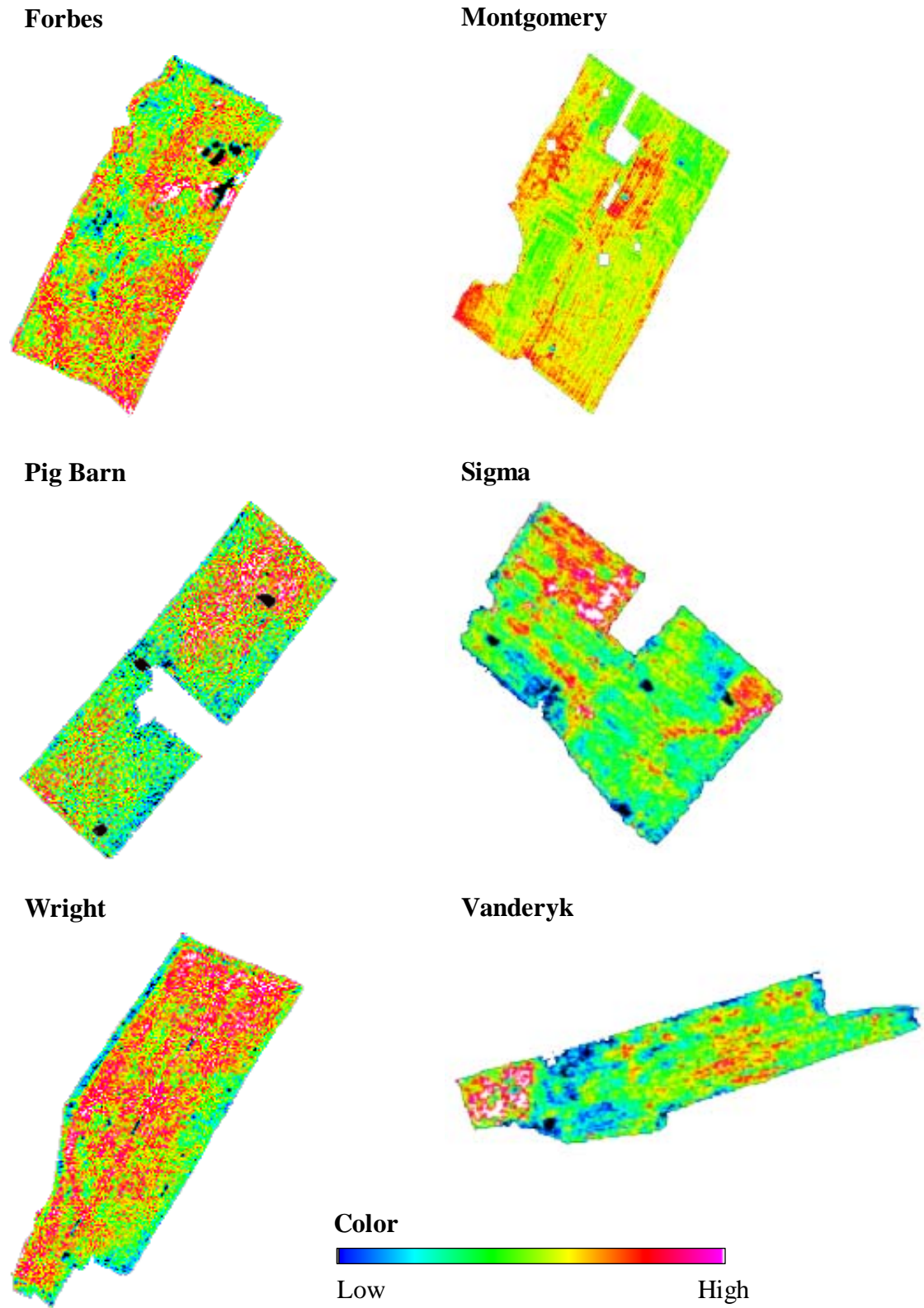## Figure 17. Chlorophyll Maps Derived From Probe-1 Hyperspectral Data

Forbes

Montgomery

Pig Barn

Sigma

Wright

Vanderyk

Color

Low   High

Table 7. Correlations Between Ground eLAI Measurements And eLAI Values Derived From The Probe-1 Hyperspectral Data

Crop Canopies	Correlation Coefficient (r)
White Bean Fields	0.16
Corn Fields	0.69*
All Canopies	0.91*

* Correlation is significant at a probability level of less than 0.05.

eLAI maps were also produced (Figure 18). Correlation coefficients were calculated for each crop type (white beans and corn) and on pooled data from all six fields. Correlations were not computed on a field-by-field basis since the number of sample points was too small and variability in eLAI values within a field was small. Only ten sample points were chosen per field and thus, more sample points would be necessary and greater variability is required to generate a valid relationship between ground eLAI and hyperpsectral eLAI values on a field-by-field basis.

The correlation coefficients generated for each crop type differ significantly. Indeed, the correlation between the ground eLAI measurements and the hyperspectral eLAI values are much higher for the corn (r = 0.69) than for the white beans (r = 0.16) (Figures 19 and 20). The difference of growth stage between the two crops was important: the three corn fields were much more developed than the white beans. Since the white bean crops were small in size, errors might have occurred when ground eLAI measurements were taken with the LAI-2000. In fact, when the LAI-2000 instrument determines eLAI values, it also estimates simultaneously a standard error for the eLAI determination (SEL). It was noted that SEL values were considerably higher for white beans. Corn fields have an average SEL value of 0.04 in comparison to 0.47 for white beans. The low correlation between ground eLAI and eLAI values derived from the hyperspectral data can also be justified by the limitations in the endmember selection. Most of the fields were using the "purest" pixels of endmembers extracted from other fields of the same crop to perform spectral unmixing. Although selecting endmembers directly from the reflectance cube itself was the best method available for endmember extraction, it could have generated some errors in the output of eLAI values from the hyperspectral data.

Finally, when all corn and white beans canopies are considered, the correlation coefficient (r = 0.91) between ground eLAI and eLAI values derived from the hyperspectral data is significant (Figure 20). Although the correlation between ground eLAI and eLAI derived from hyperspectral data is strong, errors in estimation still exist. The eLAI values derived from the remote sensing data overestimates eLAI in comparison with eLAI values measured from the LAI-2000 instrument. The range of eLAI values is also greater for eLAI estimated from hyperspectral data than from the LAI-2000 instrument. These problems can be observed on all correlation figures (Figure 19, 20 and 21). Further investigation is necessary in order to better understand eLAI estimation.

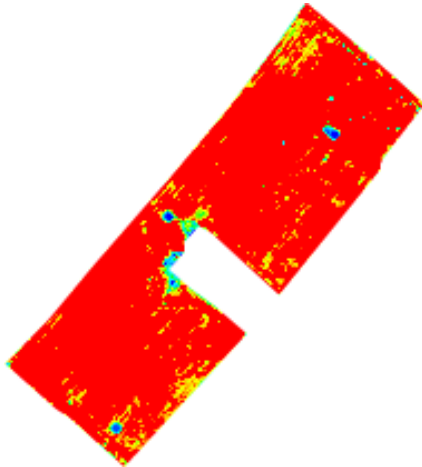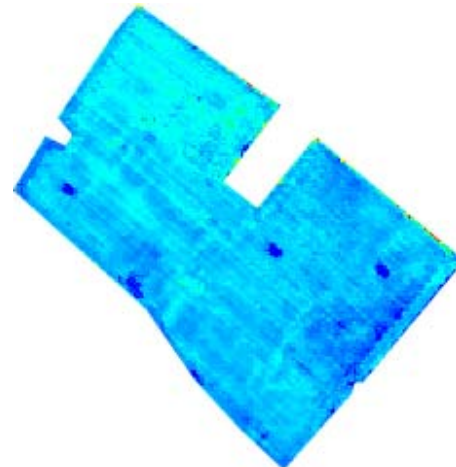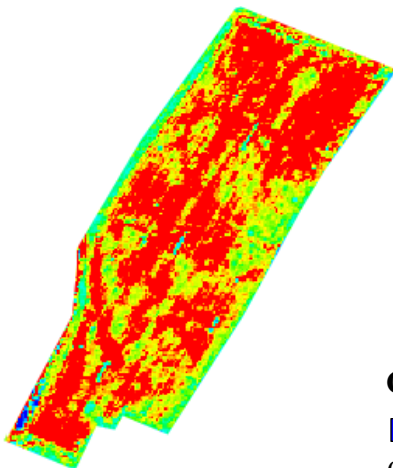### Figure 18. eLAI Maps Derived From Probe-1 Hyperspectral Data

Forbes

Montgomery

Pig Barn

Sigma

Wright

Vanderyk

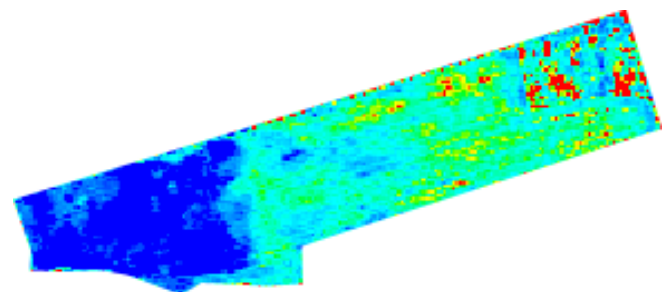**Color**

0   5
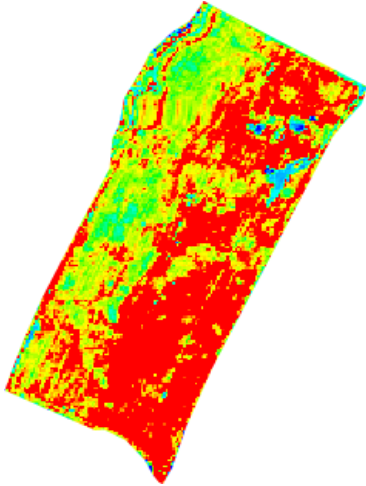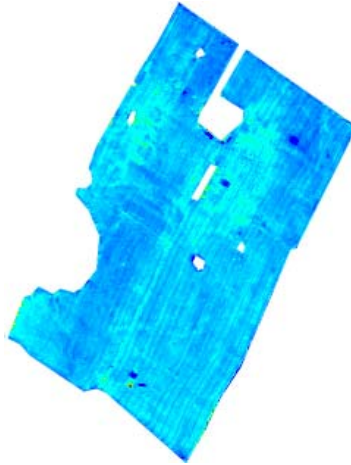
Figure 19. Correlation Between Ground eLAI Measurements And eLAI Values Derived From The Probe-1 Hyperspectral Data For White Bean Canopies
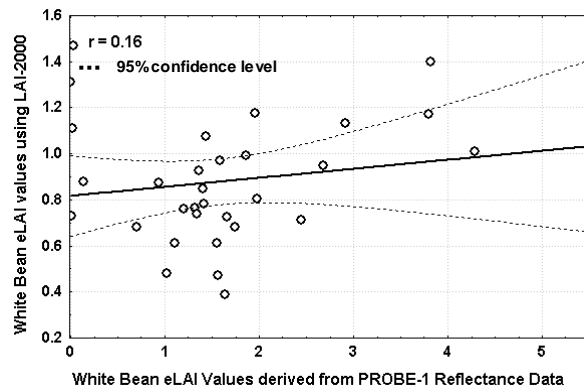

Figure 20. Correlation Between Ground eLAI Measurements And eLAI Values Derived From The Probe-1 Hyperspectral Data For Corn Canopies

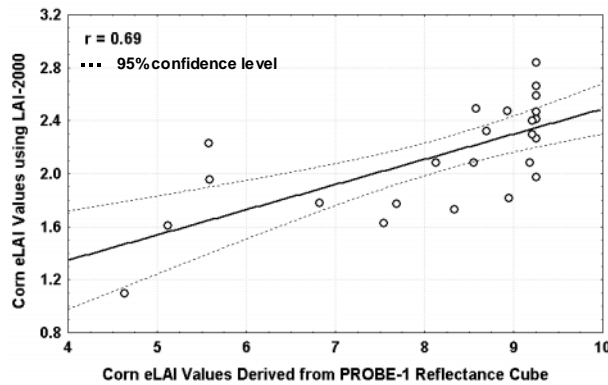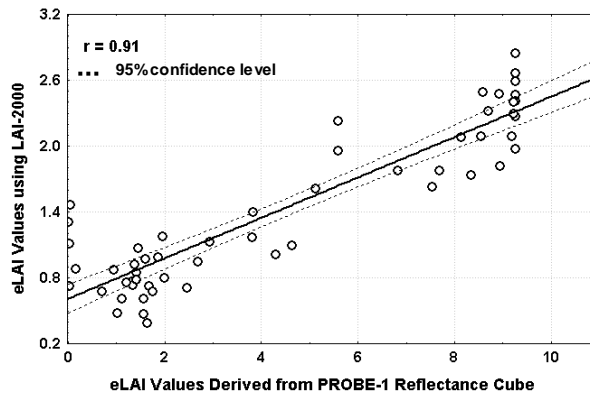**Figure 21. Correlation Between Ground eLAI Measurements And eLAI Values Derived From The Probe-1 Hyperspectral Data For White Bean And Corn Canopies**

41

Nevertheless, preliminary results are very encouraging for the estimation of eLAI from hyperspectral remote sensing data.

4.4 *Canopy Liquid Water Content*

EWT maps were derived from ISDAS and are presented in Figure 22. Further analysis is ongoing at the University of Ottawa to validate these EWT maps against ground data collected on canopy water content.

4.5 *Soil Properties*

Soil properties are also being investigated within this data set and analysis is still ongoing. Spectra from bare soil patches of all fields were extracted from the Probe-1 hyperspectral data and are being analyzed. Figure 23 illustrates the different spectra extracted and their corresponding spectral responses from 438 nm to 2506 nm. These same spectra are graphed separately for the visible and near infrared region (Figure 24) and for the mid-infrared and short wave infrared region (Figure 25). Furthermore, ground measurements such as soil moisture (%), organic matter (%) and nitrogen, extracted from these bare soil patches, are presented in Table 8.

4.6 *SAR Data Analysis*

Qualitative Observations on the Corn and White Bean Fields

Prior to any quantitative analysis, radar image composites were created using the three linear polarizations (HH, VV and HV) (Figure 26). Radar backscatter varied from field to field as a function of crop type. However, the radar imagery did not provide significant within-field precision farming scale information on the corn and white bean fields sampled during this campaign. These results can be explained by a number of factors.

Radar backscatter can vary as a function of soil and crop condition on corn fields, as demonstrated by analysis conducted on data acquired over Ottawa, Ontario (McNairn *et al.*, 2000). But radar backscatter acquired at shorter wavelengths, like C-Band, tends to saturate once large crops like corn and canola accumulate significant biomass. In the case of corn, this appears to occur at a crop height of about one metre. This suggests that for these crops, data acquired at linear polarizations (HH, VV, HV) can provide information, but only early in the growing season. In the case of the Clinton corn fields, crop height greatly surpassed one metre. As a result, in these Clinton fields corn growth across the fields appears relatively homogeneous. In the case of Pig Barn, even the Probe-1 imagery suggests relatively low variability in this field (Figure 14). For Forbes, some within field variability is evident in the radar imagery. However, the topography of this field makes it difficult to assess the influence of crop condition on radar backscatter relative to the effect of variations in local incidence angle that will also contribute to backscatter differences.

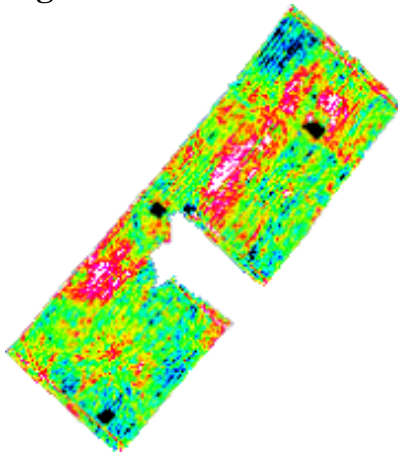## Figure 22. Liquid Water Content Maps Derived From Probe-1 Hyperspectral Data
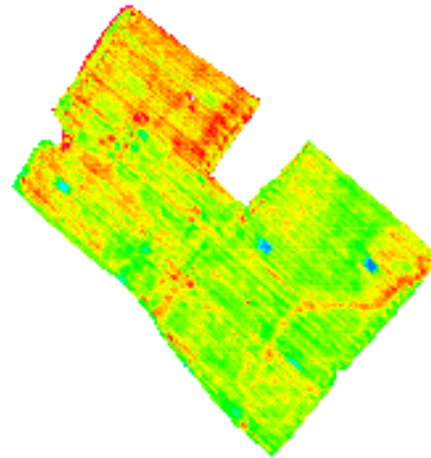
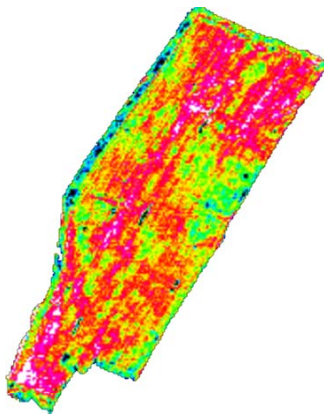**Forbes**   **Montgomery**

Pig Barn   **Sigma**

Wright   **Vanderyk**

Color Bar:

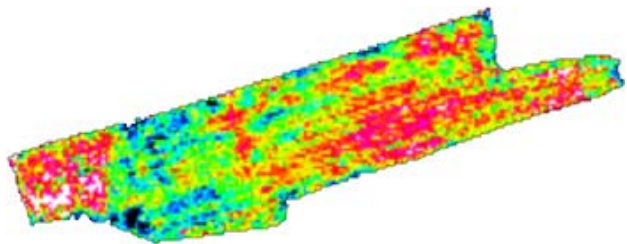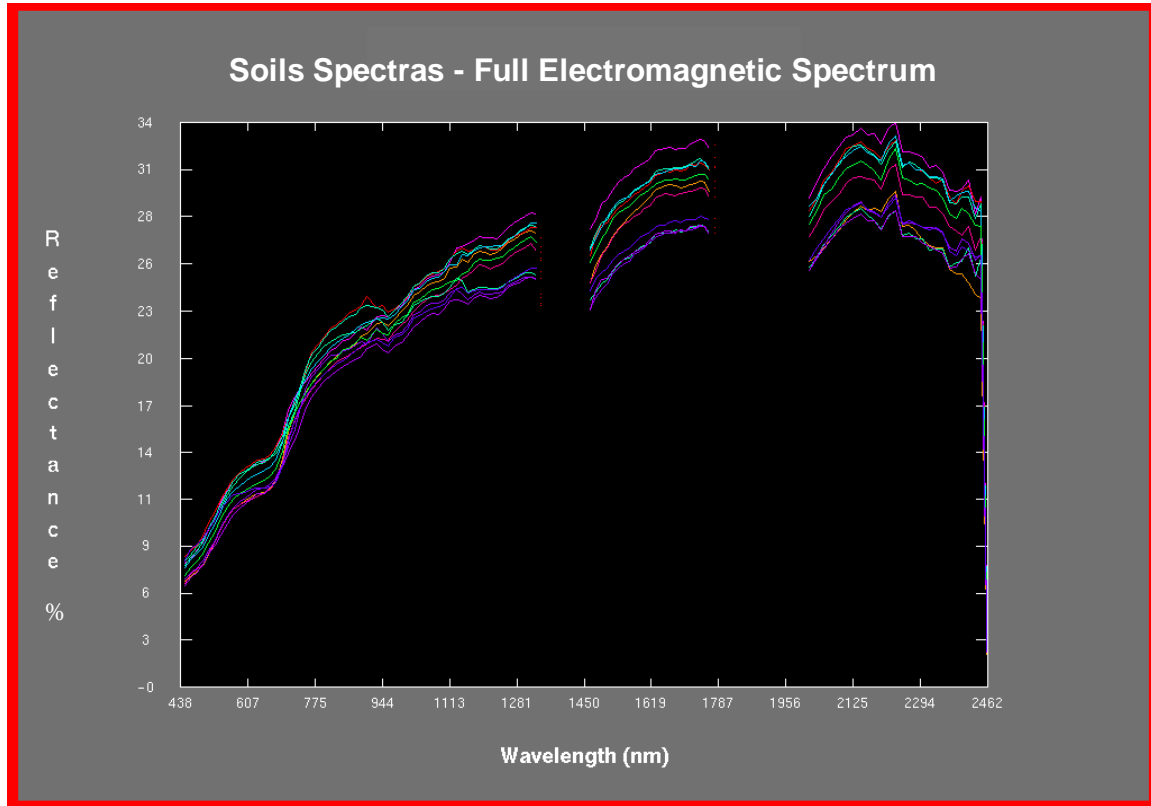Low   High
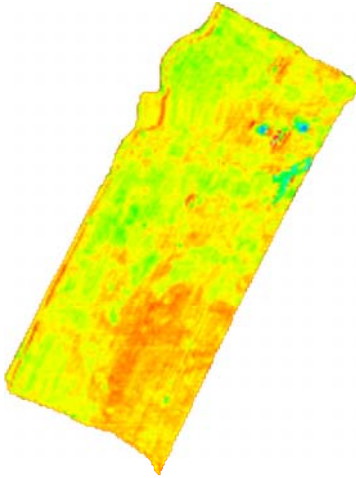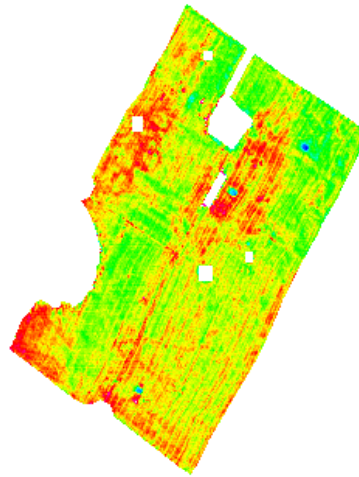
Figure 23. Soil Spectral Responses (438 – 2506 nm)

Research is continuing at CCRS to establish if other radar polarizations are less sensitive to this saturation effect and could thus provide crop condition information further into the growing season. As well, sensors that use longer wavelengths, like the L-Band PALSAR sensor scheduled for launch in 2003 on the Japanese ALOS satellite, could provide additional information.

For the three white bean fields, the radar composite did not appear to detect significant within-field variability in soil or crop conditions. This observation is also contrary to previous results reported on the Ottawa data set (McNairn *et al.*, 2000). Contrary to the corn crops, bean plants were very small and thus soil was the most dominant cover. The lack of information over the Clinton bean fields is most likely explained by the extremely dry soil conditions during the time of the SAR overflight and the low variability in soil moisture across the fields. Some moisture must be present in the target for backscatter to occur. The SAR imagery was acquired seven days prior to the Probe-1 flight. Conditions were extremely dry prior to the SAR acquisition. Rain events in the seven days between these two flights increased moisture conditions and resulted in significant crop growth. As well, bean plants were relatively small (post-emergent) during the SAR flight and thus the contribution to backscatter from these plants would also be small.

**Figure 24. Soil Spectral Responses On The Visible And Near Infrared Regions Of
The Spectrum**

Soils Spectras - Visible and NIR Spectrum
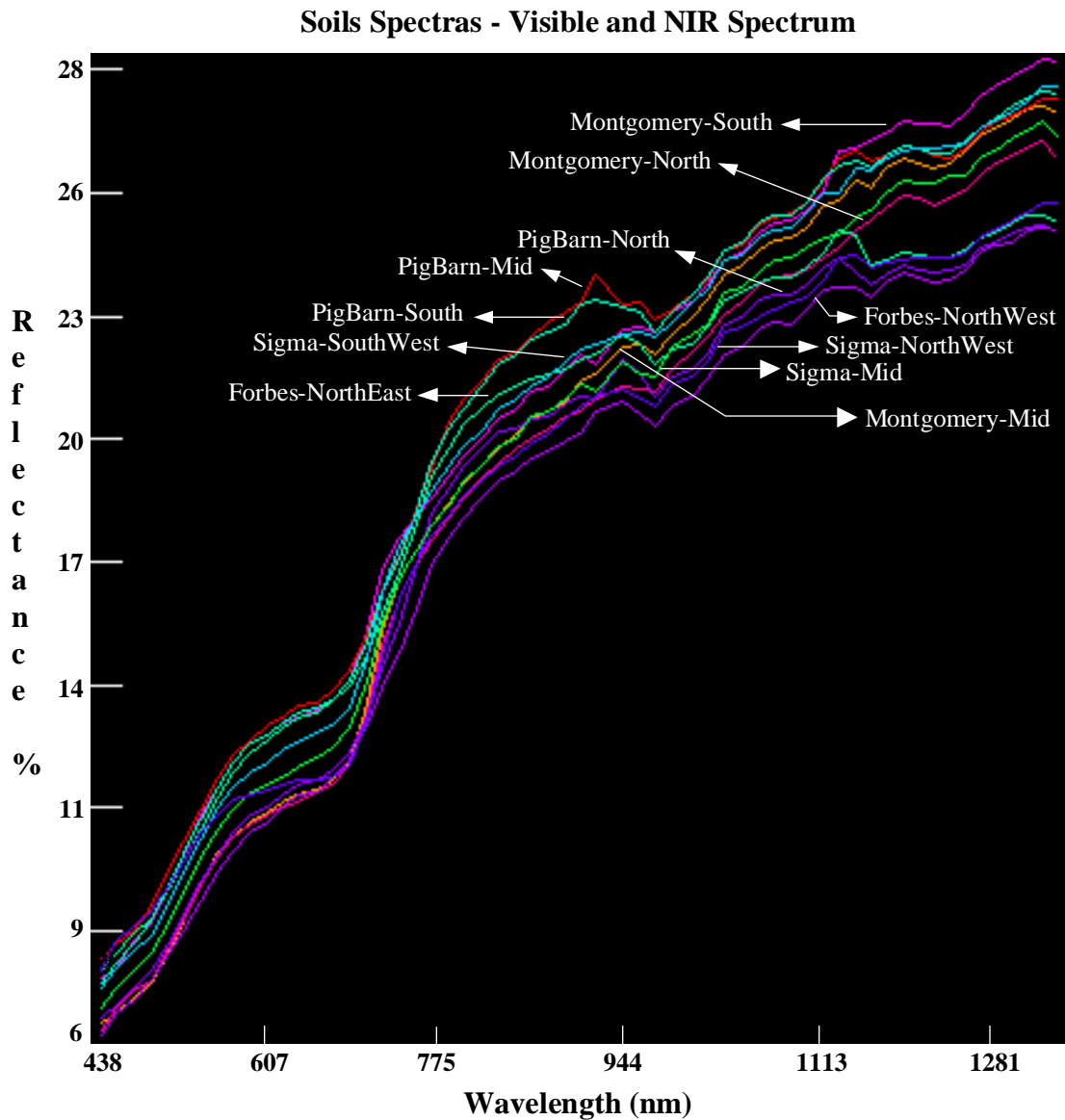
Quantitative Analysis of Wheat Fields

Although little information was found in the corn and bean fields, many small grain fields
in the area did display interesting within-field crop patterns. Barley and wheat crops
across the study site varied in their developmental stage. Most wheat crops had headed,
but fields were in various stages of senescence.

Quantitative analysis was performed on two wheat fields (one white wheat and one red
wheat) for which yield monitor data were available. The linear (HH, VV, HV) and circular

45

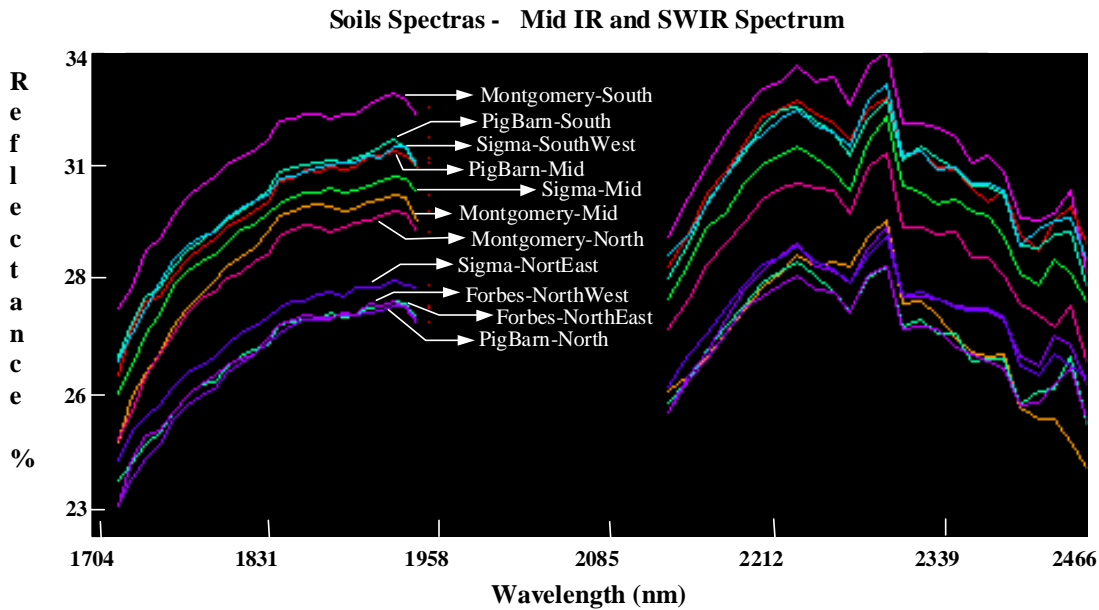**Figure 25. Soil Spectral Responses On The Mid Infrared And The Short Wave Infrared Regions Of The Spectrum**

Soils Spectras -   Mid IR and SWIR Spectrum

Table 8. Ground Measurements (Soil Moisture, Organic Matter And Nitrogen) For Each Bare Soil Patch

SOIL PROPERTIES			
	Soil Moisture (%)	Organic Matter (%)	Nitrogen
Montgomery - North	15.89	3.9	12.34
Montgomery - Mid	15.09	4.2	13.76
Montgomery - South	14.6	4.1	42
Sigma - South West	14.5	3.2	29.2
Sigma - Mid	12.43	4.2	15.3
Sigma - North East	12.99	4.3	29.6
Forbes - North East	10.63	3.2	43.52
Forbes - North West	13.61	na	na
Pig Barn - North	14.41	na	na
Pig Barn - Mid	9.64	na	na
Pig Barn - South	10.03	na	na
	Soil Moisture	Organic Matter	Nitrogen
	Max - Min	Max - Min	Max - Min
Montgomery - North	15.89		
Pig Barn - Mid	9.64		
Sigma - North East		4.3	
Sigma - South West		3.2	
Forbes - North East			43.52
Montgomery - North			12.34

Figure 26. Airborne CV-580 Radar Image Composites (R=VV, G=VH, B=HH)

Forbes (Corn)   **Montgomery (White Beans)**   **Pig Barn (Corn)**
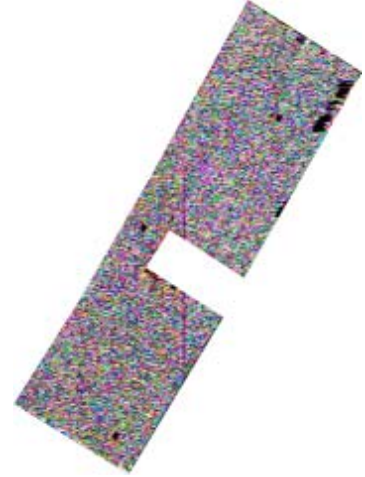
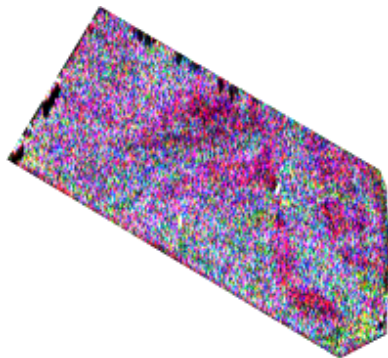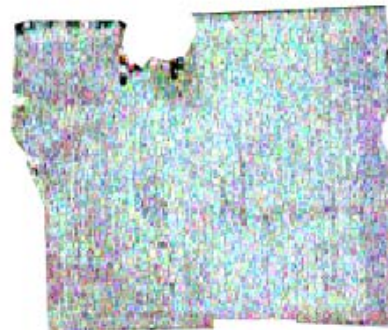**Sigma (White Beans)**   **Wright (Corn)**   **Vanderyk (White Beans)**

Eckert (Red Wheat)   **Carter (White Wheat)**

(RR, RL) polarization results are presented in this report (Figure 27). Other "polarimetric" parameters such as phase images and polarization plots were also created, but results will not be discussed. Although these parameters seem to provide some information, more research on larger data sets needs to be conducted in order to interpret this type of information and to understand the scattering mechanisms driving these parameters. As well, although RADARSAT-2 will have the capability to synthesize this type of data, operational application of these data to crop condition monitoring is unlikely in this first generation of polarimetric sensors. Most advances in SAR applications in agriculture will occur with the use of the simpler multiple linear polarization data available from RADARSAT-2.

Average backscatter for low and high yielding areas in each wheat field are presented in Figure 26. The difference in backscatter between these two zones is dependent upon polarization. For all polarizations, higher producing areas had higher backscatter relative to lower producing areas. But the linear cross-polarization (HV) gave the greatest contrast between these two zones. With the HH polarization, virtually no difference in backscatter is observed between higher and lower producing zones. However, it is difficult to compare backscatter between these two fields, since developmental stage and crop varieties were different. Thus regions of poor red wheat growth had a similar response to regions of better white wheat growth. Consequently, comparisons are limited to zones within each field.

Figure 27. Average Backscatter For Low And High Yielding Areas Of Wheat Fields
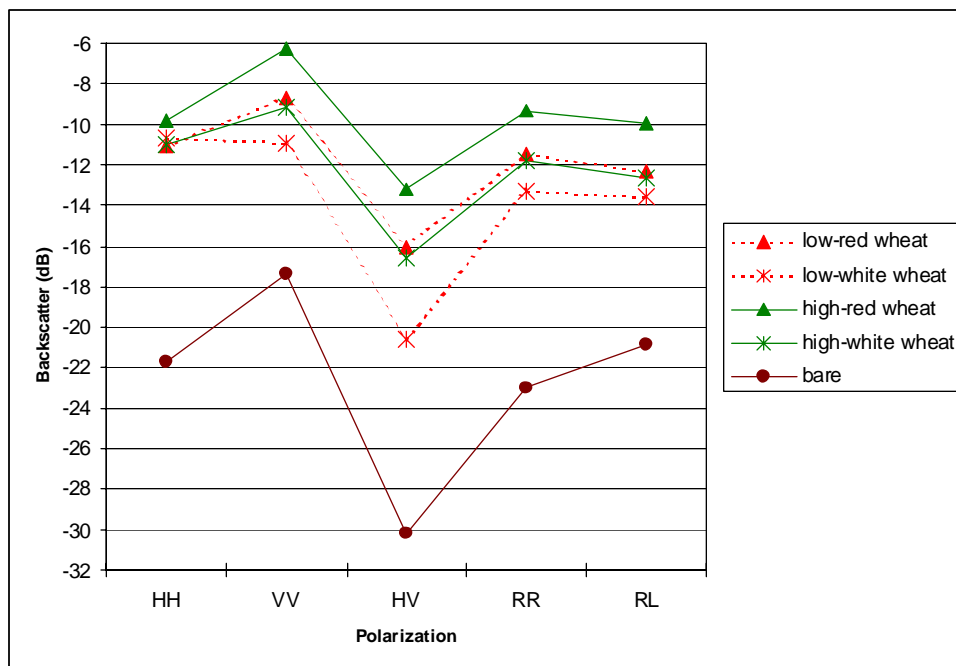
For the linear cross-polarization (HV), a 7.4 dB difference is observed between "good" red wheat and "poor" white wheat. Thus very significant variability in backscatter is associated with HV, based on both variety and crop condition. This sensitivity, although of use in crop condition mapping, complicates the use of SAR for crop type mapping. Thus a combination of polarizations that excludes HV (i.e. HH, VV, LR) and is less sensitive to within crop variability, might be better suited for crop type mapping.

Good agreement was found between the classes derived from the SAR data, and zones of productivity derived from the yield monitor data (Figure 28). Areas of high yield generally agreed with areas of high backscatter. Areas of error can be attributed to a number of factors. The SAR imagery was acquired approximately two weeks prior to harvest. Thus some changes in crop productivity may have occurred during this elapsed time. Errors also exist in the yield monitor data, primarily as a result of errors during data collection or during data processing. This is particularly evident in zones of data "misses" which exist in the yield monitor maps. Finally, crop productivity is complex and SAR data is not able to detect all of the crop and soil characteristics that determine this productivity. Nevertheless, the sensitivity of radar to wheat conditions, weeks prior to harvest, is encouraging.
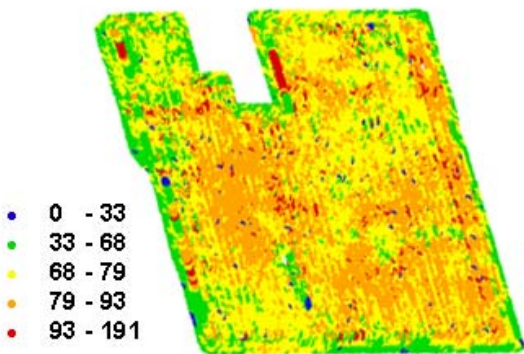
Figure 28. SAR and Yield Monitor Data For The Wheat Fields

<u>**Carter**</u>

SAR Data

<u>**Eckert**</u>

SAR Data

Yield Data

- 0 - 33
- 33 - 68
- 68 - 79
- 79 - 93
- 93 - 191

Yield Data

- 0 - 31
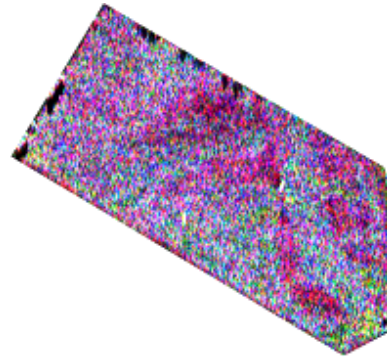- 31 - 69
- 69 - 92
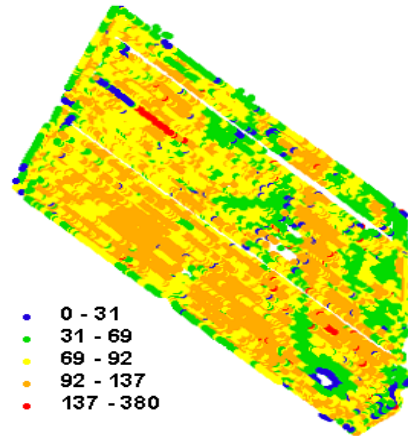- 92 - 137
- 137 - 380

SAR and Yield Agreement

Area of Agreement (Higher Yield)
Area of Agreement (Lower Yield)   ] 62%
"Error" (omission/comission)   38%

SAR and Yield Agreement

Area of Agreement (Higher Yield)
Area of Agreement (Lower Yield)   ] 77%
"Error" (omission/comission)   23%

50

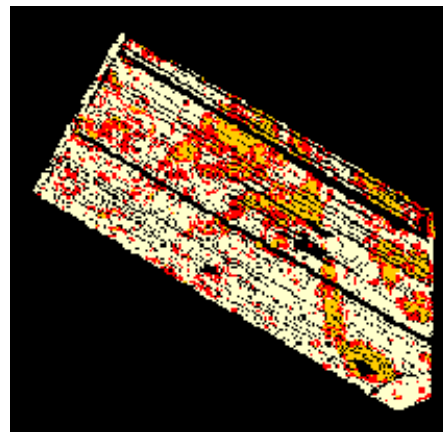5. Conclusions

Both the hyperspectral and radar imagery, acquired over the Clinton test fields, provided promising results. Two approaches were applied to the Probe-1 imagery for endmember extraction. Initially an Automatic Endmember Extraction (AEE) approach was used to derive 15 endmembers. Many of these fraction maps visually correlated with weed and disease areas delineated by the crop scouts. However, further research is required to better understand the decision regarding the optimal number of endmembers, and to interpret the endmember spectra. Manual Endmember Extraction (MEE) was the second endmember extraction approach used. With this approach, endmembers for crop, soil and residue (if present) were derived directly from the hyperspectral data. Fraction maps generated from the MEE method were correlated with percent crop cover derived from overhead ground photos. The correlation between crop fractions and percent crop cover were significant. Both endmember extraction approaches require the presence of significant patches of pure endmembers. In an operational context, these pure patches do not generally exist.

Spectral unmixing results were similar regardless of whether reflectance or radiance data were used. This observation suggests that for this purpose, atmospheric correction may not be required. Thus pre-processing requirements for operational implementation could be reduced.

Several chlorophyll extraction algorithms were tested on the Clinton data. Within a single crop type, chlorophyll variability (as estimated from SPAD-502 measurements) was low. Thus the accuracy of these techniques for within-field chlorophyll estimation could not be tested. When all data from all the fields were pooled, these algorithms could detect the differences in chlorophyll between the corn and white bean fields. However, future testing is required on data sets with greater variations in chlorophyll. Variability could be achieved by inducing differences over test sites, or by examining imagery acquired over time. These results suggest that under operational conditions it would be difficult to detect within field differences in chlorophyll from a single remote sensing acquisition.

When all data were pooled, eLAI derived from the Probe-1 imagery correlated well with eLAI values derived from an LAI-2000. Within just the white bean class, correlation results were poor. At the time of the hyperspectral acquisition, bean crops were quite small and measurement of LAI with the LAI-2000 was difficult. As with the chlorophyll methods, further validation of the LAI algorithm is required. In addition, although the algorithm was able detect areas of high and low eLAI, the algorithm greatly overestimated the absolute eLAI values. Thus further refinement of this algorithm is required.

Radar backscatter at C-Band saturates for large biomass crops like corn, once the crop reaches a height greater than one metre. Although the signature for corn is still unique relative to other crops, the radar is not able to detect within field variability related to crop condition. Very dry and uniform soil moisture conditions during the acquisition meant that the radar did not detect within field variability within the white bean fields. As well, the

bean crops were very small at the time of the SAR overflight and thus contributed little to the radar backscatter.

Yield monitor data was available for two wheat fields that exhibited significant within field differences in backscatter. Further analysis indicated that some polarizations, particularly HV, were quite sensitive to differences in productivity across these fields. Correlations between the yield monitor data, and the radar backscatter, showed good agreement. Areas of good productivity had higher backscatter relative to zones of low productivity. However, differences in backscatter were also observed between the two wheat fields as a result of differences in wheat variety. Thus information provided by radar on crop productivity needs to be interpreted on a field-by-field basis.

6. References

Blackburn, G.A. (1998), "Quantifying Chlorophylls and Carotenoids at Leaf and Canopy Scales: An evaluation of Some Hyperspectral Approaches". *Remote Sensing of Environment*, **66**: 273-285.

Boggs, J., Tsegaye, T., Fahsi, A. and T. Coleman (1998), "Assessment of Plant Nitrogen Content Using a Chlorophyll SPAD Meter and Ground Truth Data (Part I)". *First International Conference: Geospatial Information in Agriculture and Forestry*, Orlando (Florida), June 1-3, 1998, **2**: 555-559.

Chapelle, E.W., Kim, M.S. and J.E. McMurtrey III (1992), "Ratio Analysis of Reflectance Spectra (RARS): An Algorithm for the Remote Estimation of the Concentration of Chlorophyll A, Chlorophyll B, and Carotenoids in Soybean Leaves". *Remote Sensing of Environment*, **39**: 239-247.

Chen, J.M. and Cihlar, J. (1995), "Plant Canopy Gap-Size Analysis Theory for Improving Optical Measurements of Leaf Area Index", *Applied Optics*, **34**: 6211-6222.

Earth Search Sciences Inc. (2001), About Probe-1, *www.earthsearch.com/technology*.

Gao, B.-C. and A.F.H. Goetz (1990), "Column atmospheric water vapor and vegetation liquid water retrieval from Airborne Imaging Spectrometer data". *Journal of Geophysical Research*, **95**: 3549-3564.

Hawkins R. K., Touzi R. and C. E. Livingstone (1999), "Calibration and Use of CV-580 Polarimetric SAR Data". *Fourth International Airborne Remote Sensing Conference and Exhibition/21st Canadian Symposium on Remote Sensing*, Ottawa (Ontario), June 21-24, 1999.

LI-COR (1990), "Instruction Manual for LAI-2000". *LI-COR*.

McNairn, H., Brown, R. J., McGovern, M., Huffman T., and J. Ellis (2000), "Integration of Multi-Polarized Imagery for Precision Farming". *22nd Canadian Remote Sensing Symposium*, Victoria (British Columbia), August 21-25, 2000.

McNairn, H., Deguise, J.-C., and J. Secker (2001a), "Development of Remote Sensing Image Products for Use in Precision Farming". *3rd European Conference on Precision Farming*, Montpellier (France), June 18-20, 2001.

McNairn, H., Deguise, J.-C., Pacheco, A., Shang, J. and N. Rabe. (2001b), "Estimation of Crop Cover and Chlorophyll From Hyperspectral Remote Sensing". *23rd Canadian Symposium on Remote Sensing*, Quebec (Quebec), August 21-24, 2001.

Norman, J.M. (1979), "Modelling the Complete Crop Canopy". Int. B.J. Barfield and J.F. Gerber (Editors), Modification of the Aerial Environment of Plants, *American Society of Agricultural Engineers*, St. Joseph (Michigan), 249-277.

Pacheco, A., Bannari, A., Staenz, K. and H. McNairn. (2001a), "LAI Measurements in White Beans and Corn Canopies with Two Optical Instruments". *8th International Symposium – Physical Measurements and Signatures in Remote Sensing*, Aussois (France), January 8-12, 2001.

Pacheco, A., Bannari, A., Deguise, J.-C., McNairn, H. and K. Staenz (2001b), "Application of Hyperspectral Remote Sensing to the LAI Estimation in Precision Farming". *23rd Canadian Remote Sensing Symposium,* Quebec (Quebec), August 21-24, 2001.

Ross, J. (1981), "The Radiation Regime and Architecture of Plant Stands". *Dr. W. Junk Publishers*.

Secker, J., Staenz, K., Gauthier, R.P. and P. Budkewitsch (2001), "Vicarious calibration of airborne hyperspectral sensors in operational environments". *Remote Sensing of Environment*, **76**: 81-92.

Staenz, K. and D. J. Williams (1997), "Retrieval of Surface Reflectance from Hyperspectral Data Using a Look-up Table Approach". *Canadian Journal of Remote Sensing*, **23** (4): 354-368.

Staenz, K., Szeredi, T. and J. Schwarz (1998), "ISDAS – A System for Processing/ Analyzing Hyperspectral Data". *Canadian Journal of Remote Sensing*, **24** (2): 99-113.

Staenz, K., Deguise, J.-C., Chen, J.M. and H. McNairn (2001), "Estimation of Leaf Area Index (LAI) from Crop Fraction Using Hyperspectral Data". *(Submitted to the ISPRS Journal).*